

Gravitational memory meets astrophysical environments: exploring a new frontier through osculations

Rishabh Kumar Singh^{1,*}, Shailesh Kumar^{1,†}, Abhishek Chowdhuri^{2,‡} and Arpan Bhattacharyya^{1,§}

¹*Indian Institute of Technology, Gandhinagar, Gujarat-382355, India*

²*Department of Astronomy, Tsinghua University, Haidian District, Beijing 100084, China*

We study how dark matter environments influence nonlinear gravitational memory from intermediate-mass-ratio binaries. Incorporating environmental effects from the dark matter gravitational potential, dynamical friction, and accretion, we compute the leading-order nonlinear memory for both bound and unbound orbits under dark matter minispikes and Navarro-Frenk-White haloes. For quasi-circular inspirals in a minispikes, we additionally include an empirical prescription for the time-dependent evolution of the dark matter profile, which gradually evolves along the inspiral and captures the cumulative environmental response. We find that dark matter can modify the time evolution and mode content of the memory relative to the vacuum case, with the cumulative effect depending sensitively on the density profile and on how the environment accelerates the inspiral. We use these waveforms to assess signal-to-noise ratios and mismatches in representative space-based detector configurations, highlighting where memory-driven differences may be large enough to warrant targeted parameter-estimation studies. Our results emphasize that astrophysical environments can leave a hereditary imprint on gravitational memory and provide a framework for connecting memory observables with dark matter dynamics.

I. INTRODUCTION

Sources such as inspiralling binaries comprising black holes or compact objects are among the most prominent candidates for gravitational waves (GWs), providing ways to test the strong gravity regimes of black holes and astrophysical processes in extreme environments. GWs, directly detected by Earth-based observatories [1–5], have opened several new avenues in GW astronomy and further implicate the necessity of developing models for progressively complex sources with accurate precision. These models will not only provide a robust framework for testing general relativity (GR) but also will offer estimates on the detectability of GW signals by advanced Laser Interferometer Gravitational Wave Observatory (LIGO) and Laser Interferometer Space Antenna (LISA) detectors, particularly for binaries with small mass ratios. In addition to the GW signals emitted during distinct phases of binary evolution, these systems exhibit intriguing phenomena, such as gravitational/GW memory, and offer insights into environmental effects. Such aspects remain undetected in GW observations to date; however, their mutual interactions can significantly affect waveforms, enhancing their detectability through emerging observational approaches.

In this line of endeavour, the present article examines the observational consequences of an interplay between gravitational memory and the astrophysical environment. The term *gravitational memory* is a phenomenon in GR that refers to the permanent relative

change in two nearby freely falling test masses after the passage of GW [6–18]. In other words, it describes a signal that settles at a nonzero finite value rather than decaying to zero. As the wave passes through the detector setup, it distorts spacetime geometry, finally resulting in a permanent shift in the relative positions of the test masses/detectors. This intriguing area of study has recently attracted significant interest in GW physics, especially due to the potential for detection with future advanced LIGO or LISA detectors [19–26]. There is various literature available discussing numerous aspects of GW memory ranging from the conventional displacement memory effect [6–8, 27] to the kick memory by planar waves [28–34], spin memory [35, 36], memory effects in modified theories of gravity [37–42], and results from post-Newtonian (PN), self-force approaches [43, 44] and worldline effective field theory [45]. Further, recent developments have revealed a close link between the infrared structure of gravity and asymptotic symmetries that has led to the identification of the infrared triangle, which connects three fundamental ideas that were previously studied independently but now recognized to be related: *gravitational memory*, *asymptotic symmetries*, and *soft theorems* [27, 46–52]. Since our investigation focuses solely on GW memory, readers are encouraged to look at a detailed review in [27, 53] along with the references cited therein. The observational implications of the link between GW memory and asymptotic symmetries have also been examined from the perspective of numerical relativity [54–57]. GW memory is typically studied at future null infinity [27]; however, lately, an analogous memory effect has been established near the horizon of black holes, revealing a connection with asymptotic symmetries akin to the conventional memory observed at future null infinity [58–68]. It has also been shown that the nonlinear GW memory grows significantly during binary black hole mergers, with its magnitude and detectabil-

* singhrishabh@iitgn.ac.in

† shailesh.k@iitgn.ac.in; shaileshkumar.1770@gmail.com

‡ chowdhuria@tsinghua.edu.cn

§ abhattacharyya@iitgn.ac.in

ity influenced by the spin of black holes [69]. As a result, the field encompasses/offers a wide range of topics/opportunities to explore with promising possibilities of detection by future detectors.

On the other hand, the universe is permeated by a non-trivial matter medium, predominantly dark matter (DM), an enigmatic and pervasive component whose nature remains largely unknown and under active investigation. Indirect pieces of evidence support the presence of DM, albeit its exact properties continue to be unresolved and elude our understanding [70–77]. Intriguingly, in such a mystifying environment, dense matter clusters are expected to form halos, which may subsequently collapse to form black holes under the influence of gravity [75–79]. The existence of DM halos around galaxies and black holes at their centers suggests that DM can potentially impact black hole dynamics and GWs, inferring valuable insights into galactic properties. Recently, numerous studies have been conducted to analyze inspiralling and scattering binaries with distinct mass ratios in astrophysical environments and in modified gravity setups, which put forward the necessity of space-based detectors for possible detection of such an interaction from GW observations [80–99].

Further, DM environments near SMBHs can become highly concentrated as the masses of SMBHs gradually increase from 10^6 – $10^9 M_\odot$, potentially forming compact structures, called *DM spikes* [76]. While galaxy mergers and other events can disrupt DM spikes surrounding such supermassive binaries [100–104], certain structures are formed around intermediate-mass black holes (IMBHs) with masses of 10^2 – $10^5 M_\odot$, termed *minispikes* [105, 106]. GWs generated from binary black hole systems can be used to test the existence of DM minispikes as a result of their effects on the orbital dynamics of the inspiralling object [107–110]. A stellar mass object orbiting an IMBH, known as intermediate mass-ratio inspiral (IMRI), with a DM minispoke is influenced by the gravity of the central IMBH, backreaction on the object due to GW emission, DM environment, and dynamical friction (DF) [108, 111–115]. These systems also accrete, and the DF from such environments can considerably influence the evolution of IMBHs [116–118]. Therefore, a comprehensive analysis of an inspiralling binary black hole system, such as an IMRI, requires incorporating the effects of accretion alongside gravitational forces, GW backreaction, and DF [108, 114, 119–121]. Studies indicate that such effects have nontrivial impacts on the phase and can yield detectable signals from missions such as LISA, Taiji, and TianQin [108, 109]. Thus, detecting GWs from these systems could shed light on the properties of DM.

In this article, we consider elliptical, hyperbolic, and quasi-circular orbits of a stellar-mass object around the central massive black hole in an intermediate-mass-ratio (IMR) binary system immersed in a DM halo. Note that we analyze the quasi-circular case with the evolving DM minispoke profile, following [122]. Within these considerations, our main objective is to examine the interplay be-

tween gravitational memory and the DM environment, as defined by the DM minispoke and Navarro-Frenk-White (NFW) profiles. Moreover, recently in [123], it has been shown that astrophysical environments can induce transient features in GW tails and (linear) memory; however, the authors focus on linear scalar tails and memory sourced by a scalar charge, with the expectation that analogous features arise in the gravitational case. It is worth noting that our analysis adopts a distinct approach and examines the interplay between DM and nonlinear memory within the IMR framework, including the potential detectability of these two aspects by future detectors. We investigate such an interaction with the combined effects on the inspiralling object: radiation reaction, DF, and accretion phenomena. In other words, we focus on analyzing the effects of these on GW emissions resulting from orbital evolution and on the impacts of such environments on nonlinear GW memory.

For further motivation, we wish to emphasize that the environmental effects considered in this work—DM gravity, DF, and accretion—also modify the oscillatory (non-memory) part of the GW signal, primarily through changes in the orbital phase evolution, and these effects are typically larger in magnitude than their imprint on the memory itself. In other words, these effects typically enter the phase at a lower PN order and are expected to be larger in magnitude than their imprint on the memory signal. However, the purpose of the present study is not to suggest that gravitational memory provides the dominant probe of DM environments, but rather that it offers a qualitatively distinct and complementary observable. However, we know that gravitational memory is a hereditary observable that depends on the cumulative energy flux emitted over the entire past history of the binary, rather than on the instantaneous orbital dynamics. As a result, environmental effects that act over long timescales can accumulate in the GW memory in ways that differ from their effects on the oscillatory phase and amplitude. This feature makes memory particularly sensitive to long-lived astrophysical environments, such as DM minispikes surrounding IMBHs. From this perspective, studying environmental effects on memory provides a complementary probe of such effects around IMBHs. Alternatively, the presence of environments can enhance the GW memory signal relative to the vacuum case, potentially increasing its detection prospects through IMRIs. Note that a detailed analysis of parameter estimation and degeneracies associated with environmental effects in both the oscillatory waveform and memory is deferred to future work. The present analysis provides an estimate on the interplay between nonlinear memory and environmental effects.

Let us now outline the structure of the paper. In section (II), we introduce conceptual grounds of DM profiles and gravitational memory. Section (III) provides equations of motion for computing the nonlinear memory for elliptical, hyperbolic, and quasi-circular orbits, including the combined effects of DM gravity, DF, and accretion.

Section (IV) explicitly presents numerical results and the possible detectability of the interplay between memory and the DM environment with next-generation detectors. Finally, in section (V), we summarize the key findings of the study and outline the future prospects of our work.

Notation: We set the fundamental constants, gravitational constant (G) and speed of light (c) to unity.

II. SETUP: ASTROPHYSICAL ENVIRONMENT AND GW MEMORY

This section provides a brief overview of relevant DM profiles under consideration and the basics of GW memory. We then motivate the study using DM density models and describe the computational framework used to examine the interplay between GW memory and these environments.

A. Astrophysical environment

Astrophysical studies suggest that DM constitutes a major component of the universe and may form overdense regions with steep power-law profiles—DM spikes—around black holes [76]. The existence and configuration of these profiles strongly depend on the black hole’s formation history, particularly post-merger events [108]. Although such structures around supermassive black holes get depleted with time due to mergers of galaxies and other dynamical processes, they may persist around IMBHs that have not undergone any merger events in their evolutionary history [108]. Therefore, we consider central IMBHs, with masses in the range $(10^2 - 10^4)M_\odot$, embedded in DM environments. To comprehensively assess the impact of environmental conditions on GW memory, we model the surrounding DM distributions using DM minispikes and NFW profiles and analyze their effects on the system’s dynamics.

1. DM minispike profile

The DM minispike profile arises from the adiabatic growth of an IMBH within the DM halo. It is given by [108]:

$$\rho_{\text{DM}}(r) = \begin{cases} \rho_{\text{sp}} \left(\frac{r_{\text{sp}}}{r}\right)^\alpha, & r_{\text{min}} \leq r \leq r_{\text{sp}} \\ 0, & r < r_{\text{min}}, \end{cases} \quad (1)$$

B. GW memory

To reiterate, GW memory manifests itself as a lasting change in the relative separation of test masses in

where ρ_{sp} is the normalization constant and r_{sp} is empirically defined as $r_{\text{sp}} \sim 0.2r_h$ (r_h tells the gravitational influence of central IMBH), α is the DM minispike exponent, r is the distance from the center of IMBH and $r_{\text{min}} = \frac{6m_1}{c^2}$ is the innermost stable circular orbit (ISCO) distance for IMBH (m_1). The minispike exponent $\alpha = (9 - 2\alpha_{\text{in}})/(4 - \alpha_{\text{in}})$ is related to the initial inner-cusp density profile parameter α . For a minispike, $0 \leq \alpha_{\text{in}} \leq 2$ implies $2.25 \leq \alpha \leq 2.5$ [76].

2. DM NFW profile

The DM NFW profile is given as [108]:

$$\rho_{\text{DM}}(r) = \begin{cases} \frac{\rho_s}{(r/r_s)(1+r/r_s)^2}, & r_{\text{min}} \leq r \leq r_{\text{max}}, \\ 0, & r \leq r_{\text{min}} \end{cases} \quad (2)$$

where ρ_s , r_s are scaling parameters and r_{max} is the distance to which the NFW profile spreads. The NFW parameters depend on the mass of galaxy clusters and their concentration. Generally, the NFW profile is assumed as the initial DM mini-halo profile that becomes the DM minispikes after adiabatic growth of a central IMBH [108]. Here, to make the set-up clear, we consider the NFW profile as a separate individual DM environment around the IMBH and assume that its distance ranges from r_{min} to some r_{max} which is calculated based on the total mass of the DM, ρ_s and r_s as $M_{\text{DM}} = \int_{r_{\text{min}}}^{r_{\text{max}}} 4\pi r^2 \rho_{\text{DM}} dr$.

Given that DM pervades the universe, assuming binary dynamics in a vacuum is an idealization that overlooks critical environmental effects. The presence of DM influences the evolution of compact binaries and, consequently, GW memory through mechanisms such as accretion and gravitational drag, leading to deviations from the dynamics predicted under vacuum conditions. Several studies have explored these effects, typically assuming a static DM density profile [115, 118, 124]. Recently, a few attempts have been made to incorporate the dynamic density behaviour of DM using N-body simulation [125]. In this paper, we have considered the evolution of compact binaries for a static DM profile in the case of eccentric and hyperbolic orbits; however, for quasi-circular orbits, we have empirically incorporated the dynamical nature of DM density [122]. We will see that the environment significantly affects the nonlinear memory.

a detector, persisting after the GW has passed through the setup. Quantitatively, it is defined as the difference between the late and early time values of the GW polar-

TABLE I: Value of the parameters of DM profiles for central IMBH $m_1 = 10^3 M_\odot$ and total DM mass $M_{\text{DM}} = 10^6 M_\odot$ [108].

α	r_{sp}	ρ_{sp}	r_s	ρ_s	r_{min}	r_{max}
[2.25, 2.5]	0.54 pc	$226 M_\odot/\text{pc}^3$	23.1 pc	$5.61 M_\odot/\text{pc}^3$	2.96×10^{-10} pc	150.69 pc

izations:

$$\Delta h_{+, \times}^{(\text{mem})} = \lim_{t \rightarrow +\infty} h_{+, \times}(t) - \lim_{t \rightarrow -\infty} h_{+, \times}(t), \quad (3)$$

where, $h_{+, \times}$ are two GW polarizations and t is the time in the detector frame. There are two types of GW memory: (1) *Linear memory* that arises from the non-oscillatory motion of the source. It appears in unbound systems such as hyperbolic binary encounters or supernova explosions [126]. (2) *Nonlinear memory*, which originates from previously emitted GWs, which are always unbound and therefore contribute to the memory effect. This type of memory is present in all GW sources and is also known as *Christodoulou memory* [126–133]. For eccentric orbits, nonlinear memory affects the GW signal at leading-order (0PN), while for hyperbolic and parabolic orbits, it contributes at (2.5PN) order [14]. In general, we know that the GW polarizations can be expressed as the sum of multipole modes in the following way,

$$h_+ - ih_\times = \sum_{l=2}^{\infty} \sum_{m=-l}^l h^{lm} {}_{-2}\mathcal{Y}^{lm}(\Theta, \Phi), \quad (4)$$

where

$$h^{lm} = \frac{G}{\sqrt{2}Rc^{l+2}} [\mathcal{U}^{lm}(T_R) - \frac{i}{c} \mathcal{V}^{lm}(T_R)], \quad (5)$$

\mathcal{U}^{lm} and \mathcal{V}^{lm} are spherical harmonic representations of the radiative mass and current multipoles, respectively; ${}_{-2}\mathcal{Y}^{lm}(\Theta, \Phi)$ are spin-weighted spherical harmonics; T_R is the retarded time, and (R, Θ, Φ) are the distance and angles that point from the source to the observer.

In leading order, the radiative mass and the current multipoles depend on the source mass (\mathcal{I}_{lm}) and current (\mathcal{J}_{lm} , see Eq. (2.22) of [11]) multipole moments, respectively. At higher PN order, these radiative moments receive additional contributions from tail terms and other nonlinear couplings. As we are focusing on the leading-order nonlinear memory contribution, we only take into account \mathcal{U}^{lm} (there is no nonlinear memory contribution to the \mathcal{V}^{lm} , thus we neglect all current multipole moments) and neglect the higher-order terms. Under these assumptions, the waveform modes (leading-order nonlinear memory piece) become [14]:

$$h_{lm} \simeq \frac{1}{\sqrt{2}R} \mathcal{I}_{lm}^{(l)} + h_{lm}^{(\text{mem})}, \quad (6)$$

where $\mathcal{I}_{lm}^{(l)}$ is l^{th} time derivative of \mathcal{I}_{lm} and $h_{lm}^{(\text{mem})}$ is the nonlinear memory piece, given as [14]:

$$\begin{aligned} h_{lm}^{(\text{mem})} &= \frac{16\pi}{R} \sqrt{\frac{(l-2)!}{(l+2)!}} \int_{-\infty}^{T_R} dt \int d\Omega \frac{dE_{\text{GW}}}{dt d\Omega}(\Omega) \mathcal{Y}_{lm}^*(\Omega) \\ &= R \sqrt{\frac{(l-2)!}{(l+2)!}} \sum_{l'=2}^{\infty} \sum_{l''=2}^{\infty} \sum_{m'=-l'}^{l'} \sum_{m''=-l''}^{l''} (-1)^{m+m''} \\ &\quad \times \mathcal{G}_{l'l''l'm'-m''-m}^{2,-2,0} \int_{-\infty}^{T_R} dt \langle \dot{h}_{l'm'} \dot{h}_{l''m''}^* \rangle. \end{aligned} \quad (7)$$

Here $\frac{dE_{\text{GW}}}{dt d\Omega}$ is the GW flux related to h_{lm} modes, $\mathcal{G}_{l_1 l_2 l_3 m_1 m_2 m_3}^{s_1 s_2 s_3}$ is an angular ($\Omega = (\Theta, \Phi)$) integral proportional to three spin-weighted spherical harmonics [11] and $\langle \cdot \rangle$ is the average over several wavelengths of GW which is required for construction of a well-defined GW stress tensor [134].

Since the full h_{lm} modes already include the nonlinear memory term from Eq. (6), expressing the nonlinear memory modes $h_{lm}^{(\text{mem})}$ in terms of the full h_{lm} introduces a ‘nonlinear memory contribution to nonlinear memory’; however, this contribution is negligible [14]. Therefore, it is sufficient to substitute only the $\mathcal{I}_{lm}^{(l)}$ part of the h_{lm} waveform in the nonlinear memory calculation. Also, we are only concerned with the leading-order nonlinear memory piece. Therefore, we only substitute the $l=2$ modes, i.e., h_{2m} modes, on the right-hand side of Eq. (7). When $h_{lm}^{(\text{mem})}$ is expressed in terms of h_{2m} modes, one solves the angular integrals, implying certain selection rules (see Sec. III B of [11]) that will give a maximum value of ‘ l' ’ for which $h_{lm}^{(\text{mem})}$ are non-zero. So for the leading-order calculation only $h_{2m}^{(\text{mem})}$, $h_{3m}^{(\text{mem})}$ and $h_{4m}^{(\text{mem})}$ survive, and the rest of the higher- l nonlinear memory modes vanish. We can further simplify h_{lm} by only considering the non-memory piece in the following way:

$$h_{lm}^{\text{N}} \equiv \frac{\mathcal{I}_{lm}^{(l)}}{R\sqrt{2}}, \quad (8)$$

where N denotes Newtonian order and $\mathcal{I}_{lm} \propto \mathcal{Y}_{lm}^*(\theta, \phi)$ (θ and ϕ are angles in the orbital frame), resulting in $\mathcal{I}_{lm}^* = (-1)^m \mathcal{I}_{l,-m}$, $h_{lm}^* = (-1)^m h_{l,-m}$. Assuming the equatorial orbital motion, i.e., orbit lies in the x-y plane ($\theta = \pi/2$), then $h_{2,\pm 1}^{\text{N}} \propto \mathcal{Y}_{2,\pm 1}^* \propto \sin 2\theta = 0$, and then the h_{lm}^{N} modes simplify to:

$$h_{20}^{\text{N}*} = h_{20}^{\text{N}} \quad h_{2\pm 2}^{\text{N}*} = h_{2\mp 2}^{\text{N}} \quad h_{2\pm 1}^{\text{N}*} = h_{2\pm 1}^{\text{N}} = 0. \quad (9)$$

Defining $h_{lm}^{(\text{mem})(1)} = \frac{dh_{lm}^{(\text{mem})}}{dT_R}$ where angular integrals are explicitly evaluated using $\dot{h}_{lm} \rightarrow \dot{h}_{lm}^N$. Thus, after all simplifications, we obtain [14]

$$h_{2\pm 1}^{(\text{mem})(1)} = h_{3m}^{(\text{mem})(1)} = h_{4\pm 1}^{(\text{mem})(1)} = h_{4\pm 3}^{(\text{mem})(1)} = 0, \quad (10)$$

$$\begin{aligned} h_{20}^{(\text{mem})(1)} &= \frac{R}{42} \sqrt{\frac{15}{2\pi}} \langle 2|\dot{h}_{22}^N|^2 - |\dot{h}_{20}^N|^2 \rangle, \\ h_{2\pm 2}^{(\text{mem})(1)} &= \frac{R}{21} \sqrt{\frac{15}{2\pi}} \langle \dot{h}_{2\pm 2}^N \dot{h}_{20}^N \rangle, \\ h_{40}^{(\text{mem})(1)} &= \frac{R}{1260} \sqrt{\frac{5}{2\pi}} \langle |\dot{h}_{22}^N|^2 + 3|\dot{h}_{20}^N|^2 \rangle, \quad (11) \\ h_{4\pm 2}^{(\text{mem})(1)} &= \frac{R}{252} \sqrt{\frac{3}{2\pi}} \langle \dot{h}_{2\pm 2}^N \dot{h}_{20}^N \rangle, \\ h_{4\pm 4}^{(\text{mem})(1)} &= \frac{R}{504} \sqrt{\frac{14}{2\pi}} \langle (\dot{h}_{2\pm 2}^N)^2 \rangle. \end{aligned}$$

As we know, Newtonian mass multipole moments are given as:

$$\begin{aligned} \mathcal{I}_{20}^N &= -4\sqrt{\frac{\pi}{15}} \eta M r(t)^2, \\ \mathcal{I}_{2,\pm 2}^N &= 2\sqrt{\frac{2\pi}{5}} \eta M r(t)^2 e^{\mp 2i\phi(t)}, \end{aligned} \quad (12)$$

and taking their time derivatives, we can compute h_{lm}^N modes from Eq. (8) which further gives the time derivative of leading-order nonlinear memory modes $h_{lm}^{(\text{mem})(1)}$ from Eq. (11).

Thus, Sec. (II A) and (II B) naturally motivate a systematic investigation of the conceptual connection between these two notions together: astrophysical environments and nonlinear memory. Building on this framework, we demonstrate in the subsequent sections how DM minispikes can modify the cumulative nonlinear memory amplitude relative to the vacuum case, given the spike exponent. This framework motivates a systematic study of how DM minispikes modify the cumulative nonlinear memory relative to vacuum. For IMRIs observable by future space-based missions, it is then natural to ask whether these environmental modifications can produce memory signatures with astrophysically relevant signal-to-noise ratios (SNRs) in the low-frequency band, and whether the cumulative memory can encode information about the binary's evolution inside the ambient medium. This implies a nontrivial interplay between these two elusive components of the universe surrounding IMBHs. Next, we systematically examine this effect across distinct orbital configurations to assess its dependence on orbital dynamics and observables.

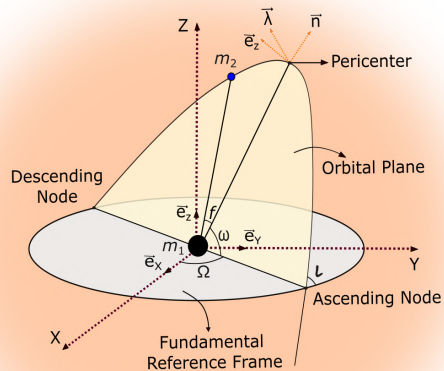


FIG. 1: Schematic of the orbital motion described in the fundamental reference frame in the presence of a surrounding DM distribution (in orange colour).

III. IMPRINTS OF ENVIRONMENT ON NONLINEAR MEMORY

In this section, we describe how we include the effects of a DM environment on top of the Newtonian equations of motion, focusing on how these effects alter the leading-order nonlinear memory term in GW signals relative to the vacuum case. We begin by formulating the perturbed Kepler problem, introducing the effects of DM, namely DM gravity, DF, and accretion, as independent perturbative forces. Each contribution is treated as a small correction to the standard Newtonian binary dynamics [135]. Using all these contributions, we derive expressions for the $h_{lm}^{\text{mem}(1)}$ modes and incorporate these effects into the orbital parameters of the binary using the osculating orbit method. The osculating orbit method is used to solve the perturbed Kepler problem, which is a set of coupled differential equations that we numerically integrate to obtain the evolution of orbital parameters, which further helps in computing the leading-order nonlinear memory for distinct orbits: elliptical, hyperbolic, and quasi-circular. In this work, we consider a non-spinning binary system with component masses $m_1 = 10^3 M_\odot$ (central IMBH) and $m_2 = 10 M_\odot$, located at a luminosity distance of $R = 10 \text{ Mpc}$ from Earth throughout our calculations.

A. Perturbed Kepler problem

The perturbation to the Kepler problem can be formulated as [135]:

$$\ddot{\vec{r}} = -\frac{M}{r^2}\hat{n} + \vec{f}, \quad (13)$$

where $\vec{r} = \vec{r}_1 - \vec{r}_2$, $r = |\vec{r}|$ is the distance between binaries and $M = m_1 + m_2$ is the total mass of the binaries. The first term in Eq. (13) is the contribution of Newtonian gravity, while the second term is due to the perturbation forces (per unit mass) to the system. A general perturbation force can be modeled as [135]:

$$\vec{f} = \mathcal{R}\hat{n} + \mathcal{S}\hat{\lambda} + \mathcal{W}\hat{e}_z, \quad (14)$$

where \mathcal{R} , \mathcal{S} , and \mathcal{W} are the components of the general perturbing force \vec{f} along the radial, tangential, and perpendicular direction to the orbital plane, respectively.

As can be intuitively understood, the presence of such perturbation forces leads to a finite change in the angular momentum vector \vec{h} (which otherwise remains conserved for a generic central force motion). The Runge-Lenz vector \vec{e}_z , too, is no longer conserved, and one can write down the time variation of these quantities in the following way [135]:

$$\begin{aligned} \frac{d\vec{h}}{dt} &= \vec{r} \times \vec{f} = -r\mathcal{W}\hat{\lambda} + r\mathcal{S}\hat{e}_z, \\ \frac{dh}{dt} &\sim r\mathcal{S}, \quad h\frac{d\vec{e}_z}{dt} = -r\mathcal{W}\hat{\lambda}. \end{aligned} \quad (15)$$

The above relations show that the changes in orbital parameters and various other dynamical quantities depend heavily on how we define the perturbing force \vec{f} . A few models motivating our scenario are discussed below.

1. DM gravity

Due to the gravitational potential of the DM density around IMBH, the stellar mass secondary BH will feel an additional force apart from the central IMBH gravity. This is termed as DM gravity and can be expressed as [107]:

$$\vec{f}_{\text{DM}} = -\frac{M_{\text{DM}}(r)}{r^2}\hat{n}, \quad (16)$$

where

$$M_{\text{DM}}(r) = \begin{cases} F \left[r^{3-\alpha} - r_{\text{min}}^{3-\alpha} \right], & \text{Minispike} \\ 4\pi\rho_s r_s^3 \left[-\frac{r}{r+r_s} + \log(r+r_s) \right. \\ \quad \left. + \frac{r_{\text{min}}}{r_{\text{min}}+r_s} - \log(r_{\text{min}}+r_s) \right], & \text{NFW} \end{cases} \quad (17)$$

and $F = \frac{4\pi\rho_{\text{sp}}r_{\text{sp}}^\alpha}{(3-\alpha)}$.

2. Dynamical Friction (DF)

A stellar-mass BH moving in a DM environment will experience gravitational drag from DM particles, perturbing its motion relative to the vacuum case. This collisionless gravitational drag is termed the Chandrasekhar DF force [111]. This DF depends on the density of the environment ρ_{DM} , the velocity of the stellar object v , and the speed of sound in the medium [112]. In the supersonic regime, the DF force per unit mass is given as [124]:

$$\vec{f}_{\text{DF}} = -\frac{4\pi m_2 \rho_{\text{DM}} I_v \xi(v)}{v^3} \vec{v}, \quad (18)$$

where $\vec{v} = \dot{r}\hat{n} + r\dot{\phi}\hat{\lambda}$ and $\xi(v) = (1-v^2)(1+v^2)^2$ account for the relativistic effect [136] and I_v is the Coulomb logarithm given as $I_v = \ln \Lambda = \ln \sqrt{m_1/m_2} \approx 3$ [108].

3. Accretion

Due to the gravity of a stellar BH, it will accrete DM matter around it. This leads to a change in the mass of a stellar object given as [116, 118]:

$$\dot{m}_2 = \frac{4\pi m_2^2 \rho_{\text{DM}} \lambda}{(v^2 + c_s^2)^{3/2}}, \quad (19)$$

where c_s is the speed of sound in the DM medium and λ is a number that depends on the medium. In this paper, we assume $\lambda = 1$ following [118]. Assuming that the accreted mass is much smaller than the mass of the stellar BH, we can model the accretion as a perturbing force per unit mass as [115]:

$$\vec{f}_{\text{acc}} \simeq \frac{\dot{m}_2 \vec{v}}{m_2} = -\frac{4\pi m_2 \rho_{\text{DM}} \lambda}{v^3} \vec{v}. \quad (20)$$

4. PN Corrections

As the binaries evolve, they will lose energy and angular momentum in the form of GW. Due to this, the binary dynamics changes and can be modeled as a perturbation force to the Newtonian binary, following [137]:

$$\vec{f}_{\text{GR}} = -\frac{M}{r^2} [\mathbf{A}\hat{n} + \mathbf{B}\vec{v}], \quad (21)$$

where

$$\begin{aligned} A_{1\text{PN}} &= -\frac{3\dot{r}^2\eta}{2} + v^2 + 3\eta v^2 - \frac{M}{r}(4+2\eta), \\ A_{2\text{PN}} &= \frac{15\dot{r}^4\eta}{8} - \frac{45\dot{r}^4\eta^2}{8} - \frac{9\dot{r}^2\eta v^2}{2} + 6\dot{r}^2\eta^2 v^2 + 3\eta v^4 \\ &\quad - 4\eta^2 v^4 + \frac{M}{r} \left[-2\dot{r}^2 - 25\dot{r}^2\eta - 2\dot{r}^2\eta^2 - \frac{13\eta v^2}{2} \right] \end{aligned} \quad (22)$$

$$+ 2\eta^2 v^2] + \frac{M^2}{r^2} \left[9 + \frac{87\eta}{4} \right], \quad (23)$$

$$A_{2.5\text{PN}} = \frac{8M\eta}{5r} \dot{r} \left[-\frac{17M}{3r} - 3v^2 \right], \quad (24)$$

$$B_{1\text{PN}} = -4\dot{r} + 2\dot{r}\eta, \quad (25)$$

$$B_{2\text{PN}} = \frac{9\dot{r}^3\eta}{2} + 3\dot{r}^3\eta^2 - \frac{15\dot{r}\eta v^2}{2} - 2\dot{r}\eta^2 v^2 + \frac{M}{r} \left[2\dot{r} + \frac{41\dot{r}\eta}{2} + 4\dot{r}\eta^2 \right], \quad (26)$$

$$B_{2.5\text{PN}} = \frac{8M\eta}{5r} \left[3\frac{M}{r} + v^2 \right], \quad (27)$$

where $M = m_1 + m_2$, $\eta = \frac{m_1 m_2}{M^2}$. Note that the effect of the GW backreaction to the binary equation of motion appears at 2.5PN order. However, in this work, we have considered all the corrections up to 2.5PN while solving the orbital evolution of binaries for the hyperbolic orbit case and only the GW backreaction term at 2.5PN for elliptic orbits. This is because the leading-order nonlinear memory for hyperbolic orbits appears at 2.5PN in the

waveform and 0PN for elliptic orbits [14].

B. Osculating orbit method

The osculating orbit method [135] provides the evolution of orbital elements, such as eccentricity, semi-latus rectum, etc., over time. For a Keplerian orbit, these quantities are constants of motion, but for a perturbed scenario, these become functions of time. Hence, the orbit equation for a perturbed Kepler orbit is given as

$$r(t) = \frac{p(t)}{1 + e(t) \cos(\phi(t) - \omega)}, \quad (28)$$

where p is the semi-latus rectum, e is the orbital eccentricity and ω is the angle of closest approach. Similarly, the rest of the orbital quantities are replaced by orbital parameters as a function of time.

$$\dot{r} = \left(\frac{M}{p(t)} \right)^{1/2} e(t) \sin(\phi(t) - \omega) ; \quad \dot{\phi} = \frac{\sqrt{Mp(t)}}{r^2}. \quad (29)$$

These evolutions of orbital elements are governed by a set of differential equations with respect to time. However, for small perturbations, we can also write these differential equations in terms of true anomaly ($f = \phi - \omega$) as an independent variable. The instantaneous osculating equations for an elliptic orbit are given as [93, 135]:

$$\begin{aligned} \frac{dp}{df} &\simeq 2\frac{p^3}{M} \frac{1}{(1 + e \cos f)^3} \mathcal{S}; & \frac{de}{df} &\simeq \frac{p^2}{M} \left[\frac{\sin f}{(1 + e \cos f)^2} \mathcal{R} + \frac{2 \cos f + e(1 + \cos^2 f)}{(1 + e \cos f)^3} \mathcal{S} \right], \\ \frac{d\iota}{df} &\simeq \frac{p^2}{M} \frac{\cos(\omega + f)}{(1 + e \cos f)^3} \mathcal{W}; & \sin \iota \frac{d\Omega}{df} &\simeq \frac{p^2}{M} \frac{\sin(\omega + f)}{(1 + e \cos f)^3} \mathcal{W}, \\ \frac{d\omega}{df} &\simeq \frac{1}{e} \frac{p^2}{M} \left[-\frac{\cos f}{(1 + e \cos f)^2} \mathcal{R} + \frac{2 + e \cos f}{(1 + e \cos f)^3} \sin f \mathcal{S} - e \cot \iota \frac{\sin(\omega + f)}{(1 + e \cos f)^3} \mathcal{W} \right], \\ \frac{dt}{df} &\simeq \sqrt{\frac{p^3}{M}} \frac{1}{(1 + e \cos f)^2} \left[1 - \frac{1}{e} \frac{p^2}{M} \left(\frac{\cos f}{(1 + e \cos f)^2} \mathcal{R} - \frac{2 + e \cos f}{(1 + e \cos f)^3} \sin f \mathcal{S} \right) \right]. \end{aligned} \quad (30)$$

For the hyperbolic orbit $e = -\frac{1}{\cos(\omega)}$, this gives the instantaneous osculating equation for a hyperbolic orbit [93, 135]:

$$\frac{de}{df} \simeq -\frac{\sin f}{\cos^2 f} \frac{d\omega}{df}, \quad (31)$$

and $\frac{dp}{df}$, $\frac{d\omega}{df}$, $\frac{dt}{df}$ are the same as mentioned above in Eq. (30). Here, \mathcal{R} , \mathcal{S} , and \mathcal{W} represent the components of the perturbing forces in a Newtonian binary system. For the type of perturbations considered in this work, the out-of-orbital-plane component \mathcal{W} vanishes (see Eq. (14)). Consequently, the orbital inclination ι and the longitude of the ascending node Ω remain constants of motion, sim-

plifying the subsequent analysis. This can be understood from Fig. (1).

C. Elliptical orbits

Having laid out the theoretical structure of our approach in this manuscript, we can now focus on specific orbital motions. In this section, we derive the leading-order nonlinear memory arising from binary interactions in elliptical orbits in the presence of non-trivial environmental contributions. We first derive $h_{lm}^{(\text{mem})}$ using the perturbed Newtonian binary equation of motion, consid-

ering DM environment effects defined in section (III A) and GW radiation reaction (2.5PN correction) because nonlinear memory appears at (0PN) in waveform [14] for elliptic orbits and also assuming contribution of other PN corrections from GR is very less compared to DM effects in elliptic orbits. Using this, we can calculate $h_{lm}^{(\text{mem})}$ by integrating with respect to eccentricity, which requires expressing other orbital parameters as functions of eccentricity. These parameters are obtained by solving the averaged osculating equations.

1. DM minispike profile \mathcal{E} memory modes

Deriving $h_{lm}^{(\text{mem})}$ for perturbed Newtonian binaries. The perturbed Newtonian binary equation, considering the effects of DM environment, including DM minispike gravity, DF, and accretion as perturbing forces from Eq.(16-20), takes the following form:

$$\ddot{\vec{r}} = -\frac{M}{r^2}\hat{n} + \vec{f}_{\text{DM}} + \vec{f}_{\text{DF}} + \vec{f}_{\text{acc}} + \vec{f}_{2.5\text{PN}}. \quad (32)$$

This equation can be resolved into components for r and ϕ using Eq. (16), (17), (18), (20) and 2.5PN correction term from sec. (III A 4) :

$$\begin{aligned} \ddot{r} &= r\dot{\phi}^2 - \frac{M_{\text{eff}}}{r^2} - \frac{F}{r^{\alpha-1}} - \frac{4\pi m_2 \rho_{\text{DM}}(I_v \xi(v) + \lambda)\dot{r}}{v^3} \\ &\quad - \frac{M}{r^2} [A_{2.5\text{PN}} + \dot{r}B_{2.5\text{PN}}], \\ \ddot{\phi} &= -\frac{2\dot{r}\dot{\phi}}{r} - \frac{4\pi m_2 \rho_{\text{DM}}(I_v \xi(v) + \lambda)\dot{\phi}}{v^3} - \frac{M}{r} [B_{2.5\text{PN}}]\dot{\phi}, \end{aligned} \quad (33)$$

where M_{eff} arises from the contribution of DM mass for the minispike profile mentioned in Eq. (17) to the total

binary mass and given as

$$M_{\text{eff}}(r) = \begin{cases} M - \frac{4\pi \rho_{\text{sp}} r_{\text{sp}}^\alpha r_{\text{min}}^{3-\alpha}}{(3-\alpha)} & , r_{\text{min}} \leq r \leq r_{\text{sp}} \\ M & , r \leq r_{\text{min}} \end{cases} \quad (34)$$

$$F = \begin{cases} \frac{4\pi \rho_{\text{sp}} r_{\text{sp}}^\alpha}{(3-\alpha)} & , r_{\text{min}} \leq r \leq r_{\text{sp}} \\ 0 & , r \leq r_{\text{min}} \end{cases} \quad (35)$$

$$\begin{aligned} \dot{r} &= \sqrt{\frac{M_{\text{eff}}}{p(t)}} e(t) \sin f(t), \\ \dot{\phi} &= \sqrt{\frac{M_{\text{eff}}}{p^3(t)}} (1 + e(t) \cos f(t))^2, \\ v &= \sqrt{\dot{r}^2 + r^2 \dot{\phi}^2}, \end{aligned} \quad (36)$$

and ρ_{DM} is the minispike density defined in Eq. (1).

Using Eq. (8) and (12), we can write expressions for h_{2m}^{N} . Then replacing \dot{r} , $\dot{\phi}$, \ddot{r} , and $\ddot{\phi}$ from Eq. (33) and (36), we obtain a lengthy and complicated expression for h_{2m}^{N} as a function of orbital parameters (e, p, ω, f). Further, taking one more time derivative of h_{2m}^{N} and a similar replacement from Eq. (33) and (36), we get \dot{h}_{2m}^{N} . We replace this long complicated¹ expression by G_{2m} , where G_{2m} is a function of (e, p, f, ω):

$$\dot{h}_{2m}^{\text{N}} \equiv \frac{\ddot{\mathcal{I}}_{2m}^{\text{N}}}{R\sqrt{2}} = G_{2m}(e, p, f, \omega). \quad (37)$$

Finally, the above equation, along with Eq. (11), gives us the time derivative of the leading-order nonlinear memory modes $h_{lm}^{(\text{mem})}$:

$$\begin{aligned} h_{20}^{(\text{mem})} &= \frac{R}{42} \sqrt{\frac{15}{2\pi}} \left\langle 2|G_{22}(e, p, f, \omega)|^2 - |G_{20}(e, p, f, \omega)|^2 \right\rangle, \\ h_{2\pm 2}^{(\text{mem})} &= \frac{R}{21} \sqrt{\frac{15}{2\pi}} \left\langle G_{2\pm 2}(e, p, f, \omega) G_{20}(e, p, f, \omega) \right\rangle, \\ h_{40}^{(\text{mem})} &= \frac{R}{1260} \sqrt{\frac{5}{2\pi}} \left\langle |G_{22}(e, p, f, \omega)|^2 + 3|G_{20}(e, p, f, \omega)|^2 \right\rangle, \\ h_{4\pm 2}^{(\text{mem})} &= \frac{R}{252} \sqrt{\frac{3}{2\pi}} \left\langle G_{2\pm 2}(e, p, f, \omega) G_{20}(e, p, f, \omega) \right\rangle, \\ h_{4\pm 4}^{(\text{mem})} &= \frac{R}{504} \sqrt{\frac{14}{2\pi}} \left\langle (G_{2\pm 2}(e, p, f, \omega))^2 \right\rangle. \end{aligned} \quad (38)$$

¹ For all the lengthy calculations, we have used the Python symbolic calculation package SymPy to reduce the labor of writing

big expressions used in further calculations. Also, we don't show

Note that after simplifying the above expression, we observe that only $\{2, \pm 2\}$, $\{4, \pm 2\}$, and $\{4, \pm 4\}$ are functions of e , p , f , and ω . The $\{2, 0\}$ and $\{4, 0\}$ do not explicitly depend on ω , and are just functions of e , p , and f . This will further help our calculation of dominant leading-order nonlinear memory modes, i.e. $\{2, 0\}$ and $\{4, 0\}$.

Calculating nonlinear memory. To obtain $h_{lm}^{(\text{mem})}$ from Eq. (38) for an elliptical orbit, we resort to averaging over the orbital period of the binary T_{orb} . The orbital-averaging formula for any function $F(t)$ is given as:

$$\begin{aligned} \langle F(t) \rangle &= \frac{1}{T_{\text{orb}}} \int_0^{T_{\text{orb}}} F(t) dt, \\ &= \frac{(1-e^2)^{3/2}}{2\pi} \int_0^{2\pi} df \frac{F(f)}{(1+e \cos f)^2}, \end{aligned} \quad (39)$$

where t is the time, f is the true anomaly and e is the orbital eccentricity. Owing to the complicated expression of $h_{lm}^{(\text{mem})(1)}$ in Eq. (38), we resort to computing the average numerically and define the numerical function to be H , which depends on (e, p, ω) .

$$h_{lm}^{(\text{mem})(1)} = H(e, p, \omega). \quad (40)$$

This averaging technique eliminates the high-frequency component from the memory waveform [14] and also implies an adiabatic approximation, i.e. the time scale on which orbital parameters change is much larger than the orbital period [138, 139]. Such approximations are valid in our cases since the perturbations to the Newtonian binary are very small.

Given the numerical solution of the above Eq. (40), we use it to compute a time integral to get $h_{lm}^{(\text{mem})}$. Since orbital parameters e , p , and ω are functions of true anomaly due to the perturbing forces, their instantaneous evolution is governed by osculating equations Eq. (30). Using adiabatic approximation, we can thus write the averaged osculating equations and solve this set of coupled differential equations given as:

$$\begin{aligned} \left\langle \frac{dp}{df} \right\rangle &= \left\langle \frac{dp}{df} \right\rangle_{\text{DM}} + \left\langle \frac{dp}{df} \right\rangle_{\text{DF}} + \left\langle \frac{dp}{df} \right\rangle_{\text{acc}} + \left\langle \frac{dp}{df} \right\rangle_{\text{GW}}, \\ \left\langle \frac{de}{df} \right\rangle &= \left\langle \frac{de}{df} \right\rangle_{\text{DM}} + \left\langle \frac{de}{df} \right\rangle_{\text{DF}} + \left\langle \frac{de}{df} \right\rangle_{\text{acc}} + \left\langle \frac{de}{df} \right\rangle_{\text{GW}}, \\ \left\langle \frac{d\omega}{df} \right\rangle &= \left\langle \frac{d\omega}{df} \right\rangle_{\text{DM}} + \left\langle \frac{d\omega}{df} \right\rangle_{\text{DF}} + \left\langle \frac{d\omega}{df} \right\rangle_{\text{acc}} + \left\langle \frac{d\omega}{df} \right\rangle_{\text{GW}}, \\ \left\langle \frac{dt}{df} \right\rangle &= \left\langle \frac{dt}{df} \right\rangle_{\text{DM}} + \left\langle \frac{dt}{df} \right\rangle_{\text{DF}} + \left\langle \frac{dt}{df} \right\rangle_{\text{acc}} + \left\langle \frac{dt}{df} \right\rangle_{\text{GW}}, \end{aligned} \quad (41)$$

where $\langle \rangle_{\text{DM}}$, $\langle \rangle_{\text{DF}}$, $\langle \rangle_{\text{acc}}$, and $\langle \rangle_{\text{GW}}$ are averaged osculating equations due to DM gravity, DF, accretion, and

GW backreaction perturbation, respectively. We numerically solve these coupled differential equations starting from an initial eccentricity e_0 and semi-latus rectum p_0 till the secondary reaches the last stable orbit (LSO).

Using the solution of Eq. (41), we numerically integrate the nonlinear memory modes as a function of eccentricity using the Euler method:

$$h_{lm}^{(\text{mem})} = \int_{-\infty}^{T_R} h_{lm}^{(\text{mem})(1)} dt = \int_{e_0}^{e(t)} h_{lm}^{(\text{mem})(1)} \frac{\langle \frac{dt}{df} \rangle}{\langle \frac{de}{df} \rangle} de. \quad (42)$$

A similar procedure is adopted for the NFW profile to compute the leading-order nonlinear memory modes. The only modification lies in the DM gravitational force term appearing in the perturbed equations of motion, as detailed in the Appendix (A).

D. Hyperbolic orbits

In this section, we derive the leading-order nonlinear memory arising from binaries in scattering/hyperbolic orbits in a DM environment. Similar to the elliptical orbit case, we first derive $h_{lm}^{(\text{mem})(1)}$ using the perturbed Newtonian binary equation of motion, but here we consider both the DM environment as well as PN corrections to orbital equations up to 2.5PN order defined in section (III A) because nonlinear memory contribution appears at 2.5PN in waveforms for hyperbolic orbits. Thus, we cannot neglect the PN corrections to the orbit equation up to 2.5PN [14]. We calculate $h_{lm}^{(\text{mem})}$ by integrating with respect to the true anomaly variable, which requires expressing other orbital parameters as functions of true anomaly which can again be obtained by solving the instantaneous osculating equations for the hyperbolic case following Eq. (31).

1. DM minispikes profile: memory modes and ‘‘jump’’

Deriving $h_{lm}^{(\text{mem})(1)}$ for perturbed Newtonian binaries. For the hyperbolic case, in the perturbed Newtonian binary equations that we are setting up, we include the effects of DM environment and PN corrections up to 2.5PN terms as perturbing forces (16-27):

$$\ddot{\vec{r}} = -\frac{M}{r^2} \hat{n} + \vec{f}_{\text{DM}} + \vec{f}_{\text{DF}} + \vec{f}_{\text{acc}} + \vec{f}_{\text{GR}}. \quad (43)$$

Resolving these equations into components, we get,

those expressions explicitly in the manuscript as they are not very illuminating.

$$\begin{aligned}\ddot{r} &= r\dot{\phi}^2 - \frac{M_{\text{eff}}}{r^2} - \frac{F}{r^{\alpha-1}} - \frac{4\pi m_2 \rho_{\text{DM}}(I_v \xi(v) + \lambda) \dot{r}}{v^3} - \frac{M}{r^2} \left[(A_{1\text{PN}} + A_{2\text{PN}} + A_{2.5\text{PN}}) + \dot{r}(B_{1\text{PN}} + B_{2\text{PN}} + B_{2.5\text{PN}}) \right], \\ \ddot{\phi} &= -\frac{2\dot{r}\dot{\phi}}{r} - \frac{4\pi m_2 \rho_{\text{DM}}(I_v \xi(v) + \lambda) \dot{\phi}}{v^3} - \frac{M}{r} \left[B_{1\text{PN}} + B_{2\text{PN}} + B_{2.5\text{PN}} \right] \dot{\phi}.\end{aligned}\tag{44}$$

Following similar steps described in section (III C 1), we can write the time derivative of the leading-order nonlinear memory modes $h_{lm}^{(\text{mem})(1)}$ as a function K_{2m} (owing

to the complicated expression) depending on e , p , f and ω [14]:

$$\begin{aligned}h_{20}^{(\text{mem})(1)} &= \frac{R}{42} \sqrt{\frac{15}{2\pi}} \left\langle 2|K_{22}(e, p, f, \omega)|^2 - |K_{20}(e, p, f, \omega)|^2 \right\rangle, \\ h_{2\pm 2}^{(\text{mem})(1)} &= \frac{R}{21} \sqrt{\frac{15}{2\pi}} \left\langle K_{2\pm 2}(e, p, f, \omega) K_{20}(e, p, f, \omega) \right\rangle, \\ h_{40}^{(\text{mem})(1)} &= \frac{R}{1260} \sqrt{\frac{5}{2\pi}} \left\langle |K_{22}(e, p, f, \omega)|^2 + 3|K_{20}(e, p, f, \omega)|^2 \right\rangle, \\ h_{4\pm 2}^{(\text{mem})(1)} &= \frac{R}{252} \sqrt{\frac{3}{2\pi}} \left\langle K_{2\pm 2}(e, p, f, \omega) K_{20}(e, p, f, \omega) \right\rangle, \\ h_{4\pm 4}^{(\text{mem})(1)} &= \frac{R}{504} \sqrt{\frac{14}{2\pi}} \left\langle (K_{2\pm 2}(e, p, f, \omega))^2 \right\rangle.\end{aligned}\tag{45}$$

Nonlinear memory and the “jump”. While integrating the above expressions for $h_{lm}^{(\text{mem})}$ as a function of true anomaly f , we can also compute an overall “nonlinear memory jump” $\Delta h_{lm}^{(\text{mem})}$ owing to the periastron passage which happens very quickly for hyperbolic encounter. This nonlinear memory jump can be obtained as a function of different initial eccentricities e_0 ’s. Consequently, different values of e_0 correspond to different values of the overall nonlinear memory jump for the whole orbit.

Since an unbound orbit is not periodic, an averaging procedure of the type used for elliptical orbits is not applicable. We can only integrate expressions in Eq. (45) with respect to time to obtain $h_{lm}^{(\text{mem})}$. While doing so, we need to change variables from time t to true anomaly f using the instantaneous osculating equation for hyperbolic orbits in Eq. (31) and replace e , p , and ω as functions of f , which comes after numerically solving the instantaneous osculating equations. Therefore, integrating expressions in Eq. (45) with respect to f from initial angle $f_{\text{in}} = \cos^{-1}(-\frac{1}{e_0})$ (correspond to a situation when the binaries are very far apart, ideally $-\infty$) to a value $f(t)$ at a later time. We can then write $h_{lm}^{(\text{mem})}$ as [14]:

$$h_{lm}^{(\text{mem})} = \int_{-\infty}^{T_R} h_{lm}^{\text{mem}(1)} dt = \int_{f_{\text{in}}}^{f(t)} h_{lm}^{\text{mem}(1)} \frac{dt}{df} df.\tag{46}$$

We can then define an overall nonlinear memory “jump” as an integration from f_{in} to f_{final} , which corresponds

to binaries that start from very far away (ideally $-\infty$) distance will go to far away (ideally ∞) after the whole hyperbolic encounter [14]:

$$\Delta h_{lm}^{(\text{mem})} = \int_{f_{\text{in}}}^{f_{\text{final}}} h_{lm}^{\text{mem}(1)} \frac{dt}{df} df.\tag{47}$$

In order to compute this jump, we consider the instantaneous osculating equations for the hyperbolic case, Eq. (31), considering all DM environment effects and PN corrections up to 2.5PN (which can be written using the perturbing force expressions from Eq. (16-27)) and solve this set of differential equations numerically [140]². This gives the orbital quantities (e, p, ω) as a function of f , and when one puts these quantities back into the above Eq. (46-47), it gives us the nonlinear memory and overall memory jump for the hyperbolic orbit case. Again, using the same methodology, we compute the nonlinear memory modes for the NFW profile, employing the corresponding equations of motion given in the Appendix (A). In the next section, we will conduct a comparative study of the nonlinear memory embedded in these two different static DM environments, i.e., the DM spike and NFW models for hyperbolic orbits.

² The Github repository of our detailed code can be found here [140].

E. Quasi-circular orbits

In the previous section, we have considered the evolution of the binary assuming a static density profile of DM around the IMBH. However, in a more realistic scenario, the DM distribution itself may evolve in response to changes in the orbital parameters of the binary. This coupled evolution is driven by GW emission and DF exerted by the DM dress surrounding the lighter compact object (m_2) [122]. Motivated by the qualitative estimate of the evolution of the DM distribution for circular binaries—accounting only for GW backreaction and DF, as discussed in Sec. IV of Ref. [122]—we introduce an empirical effective DM density profile (EDP) around the IMBH that approximately captures this behavior. We used this profile to calculate leading-order nonlinear memory arising from binaries in quasi-circular orbits (low eccentric orbits, nearly circular). We start with an initial density of DM minispikes profile and then empirically evolve it as the binary evolves over time [122]. The scenario described by EDP around quasi-circular binary that experiences GW backreaction and DF from the DM spike environment. Quasi-circular binaries start evolving in such an environment, and with time, they reach a break point r_b , the distance corresponding to the dephasing break frequency f_b [122]. We assume that this distance r_b corresponds to the critical radius p_c [115], where the eccentricity growth from the DF balances the eccentricity decay from GW backreaction. At distances greater than r_b , the EDP drops according to $\rho_{\text{DM}}(r \gg r_b) \propto r^{-(\alpha+\gamma)}$, where γ is nearly independent of the DM parameters. And at small separations ($r \ll r_b$), the EDP approaches its initial $\rho_{\text{DM}}(r, t = 0) \propto r^{-\alpha}$. To analytically model this qualitative assessment, we are writing an EDP profile as [122]:

$$\rho_{\text{DM}}(r) = \rho_{\text{sp}} \left(\frac{r_{\text{sp}}}{r} \right)^{\alpha+\gamma(\kappa)}, \quad r_{\text{ISCO}} < r < r_{\text{sp}}. \quad (48)$$

Here, we model γ as a function of separation r through κ such that γ starts from 0 at $r = 0$ and reaches a peak value at $r = r_b$ and finally goes down to 0 again at small separations ($r \ll r_b$). This feature is empirically cap-

tured by assuming $\gamma(\kappa)$ to be defined as:

$$\gamma(\kappa) = (2.5 - \alpha) e^{-(\kappa(r) - \kappa_{\text{max}})^2}, \quad (49)$$

where

$$\kappa(r) = \kappa_f \frac{(r - r_{\text{init}})}{(r_{\text{ISCO}} - r_{\text{init}})}, \quad (50)$$

and κ_{max} corresponds κ at $r = r_b$, and factor $(2.5 - \alpha)$ is there to keep the DM minispikes exponent to be in the range $[2.25, 2.5]$ following [76] and we set $\kappa_f = 10$ (or any large positive number will also work) so that the EDP follows the initial DM minispikes profile for $r \ll r_b$.

Since we are focusing on circular binaries, i.e., binaries with eccentricity $e \sim 0$, we can have an estimate by analytically expanding our previously obtained complicated expressions in a small eccentricity expansion (hence, the word “quasi-circular”). With this model of evolving DM density, which depends on binary separation, the perturbed binary equations for a quasi-circular orbit look like:

$$\ddot{\vec{r}} = -\frac{M}{r^2} \hat{n} + \vec{f}_{\text{DF}} + \vec{f}_{2.5\text{PN}}. \quad (51)$$

This equation can again be resolved into r and ϕ motions:

$$\begin{aligned} \ddot{r} &= r\dot{\phi}^2 - \frac{M}{r^2} - \frac{4\pi m_2 \rho_{\text{DM}} I_v \xi(v) \dot{r}}{v^3} - \frac{M}{r^2} [A_{2.5\text{PN}} + \dot{r} B_{2.5\text{PN}}], \\ \ddot{\phi} &= -\frac{2\dot{r}\dot{\phi}}{r} - \frac{4\pi m_2 \rho_{\text{DM}} I_v \xi(v) \dot{\phi}}{v^3} - \frac{M}{r} [B_{2.5\text{PN}}] \dot{\phi}. \end{aligned} \quad (52)$$

Using the above equation of motion and following a similar procedure as in the elliptical case, we can express the first time derivative of the nonlinear memory mode $h_{lm}^{(\text{mem}) (1)}$. To compute the nonlinear memory, we integrate over eccentricity as given in Eq. (42) which requires the evolution of the orbital parameters ($e(f), p(f), \omega(f), t(f)$) (we obtain these by solving the averaged osculating equations for a quasi-circular binary). While writing the instantaneous osculating equations we perform a small eccentricity expansion keeping terms $\sim \mathcal{O}(e^4)$ followed by an orbital averaging over the whole time period of motion of the binary to obtain the averaged osculating equation³:

³ For $\langle \frac{de}{df} \rangle_{\text{quasi}}$, the next higher-order term appears at e^5 .

$$\begin{aligned}
\left\langle \frac{de}{df} \right\rangle_{\text{quasi}} &= -\frac{\eta}{15} \left(\frac{M}{p} \right)^{5/2} e (304 + 121e^2) + \frac{\pi I_v m_2 \rho_{sp}}{2M^2} \left(\frac{r_{sp}}{p} \right)^\alpha \left\{ 4e \left[(\alpha + 3)M^3 + (\alpha + 1)M^2p - (\alpha - 1)Mp^2 \right. \right. \\
&\quad \left. \left. - (\alpha - 3)p^3 \right] - e^3 \left[(\alpha + 3)(\alpha^2 + \alpha + 3)M^3 + (\alpha + 1)(\alpha^2 - 3\alpha + 3)M^2p - (\alpha - 1)(\alpha^2 - 7\alpha + 11)Mp^2 \right. \right. \\
&\quad \left. \left. - (\alpha - 3)(\alpha^2 - 11\alpha + 27)p^3 \right] \right\}, \\
\left\langle \frac{dp}{df} \right\rangle_{\text{quasi}} &= -\frac{8\eta}{5} \left(\frac{M}{p} \right)^{5/2} p (8 + 7e^2) + \frac{\pi I_v m_2 p \rho_{sp}}{8M^2} \left(\frac{r_{sp}}{p} \right)^\alpha \left\{ \mathcal{A}_1(M, p) + e^2 \mathcal{A}_2(M, p, \alpha) - e^4 \mathcal{A}_3(M, p, \alpha) \right\}, \\
\left\langle \frac{d\omega}{df} \right\rangle_{\text{quasi}} &= 0, \\
\left\langle \frac{dt}{df} \right\rangle_{\text{quasi}} &= \left(\frac{p}{M} \right)^{1/2} \frac{p}{4} (8 + 12e^2 + 15e^4),
\end{aligned} \tag{53}$$

where

$$\mathcal{A}_1 = 64M^3 + 64M^2p - 64Mp^2 - 64p^3, \tag{54}$$

$$\mathcal{A}_2 = 16(\alpha^2 + \alpha + 3)M^3 + 16((\alpha - 3)\alpha + 3)M^2p - 16((\alpha - 7)\alpha + 11)Mp^2 - 16((\alpha - 11)\alpha + 27)p^3, \tag{55}$$

$$\begin{aligned} \mathcal{A}_3 &= (\alpha(\alpha((\alpha - 2)\alpha + 5) - 16) + 21)M^3 + (\alpha(\alpha((\alpha - 10)\alpha + 37) - 64) + 45)M^2p \\ &\quad - (\alpha(\alpha((\alpha - 18)\alpha + 117) - 320) + 309)Mp^2 - (\alpha(\alpha((\alpha - 26)\alpha + 245) - 976) + 1389)p^3. \end{aligned} \tag{56}$$

Solving this set of differential equations numerically gives the evolution of orbital parameters, which we use to solve the integral in Eq. (42) to obtain nonlinear memory for a quasi-circular orbit in an evolving DM environment. In the next section, we will conduct a comparative study of the nonlinear memory embedded in this evolving DM minispikes and static profiles with vacuum for quasi-circular orbits.

IV. NUMERICAL RESULTS AND DETECTION PROSPECTS

In this section, we present our results and estimate the prospects for the detection nonlinear GW memory using space-based detectors such as LISA and GWSat. We plot the nonlinear memory as a function of eccentricity for an elliptical orbit, first considering only the GW backreaction (only 2.5PN term) for the vacuum case (without DM) and then the net effect (with DM), including DM gravity, DF, accretion, and GW backreaction. We also plot the nonlinear memory as a function of true anomaly for a hyperbolic orbit, considering PN correction terms up to 2.5PN (without DM) and the net effect. Both plots highlight the hereditary nature of nonlinear memory build-up. Note that we consider a binary located at a distance of $R = 10$ Mpc.

Further, to assess detectability, we numerically computed the SNR for both the LISA and GWSat detectors and found that the signals are detectable in both cases

within the present approximations for elliptical binaries. However, distinguishing whether a detected signal originates from a binary evolving in vacuum or within a DM environment is expected to be highly challenging. Beyond detectability, the SNR analysis also provides insight into how DM influences the nonlinear GW memory by plotting the SNR of the memory signal in vacuum and in DM for various values of the DM exponent (α). In addition, we computed the waveform mismatch to quantify the impact of memory on signals from binaries embedded in a DM environment around an IMBH. This analysis was carried out using the stationary phase approximation (SPA) for waveforms from low-eccentricity elliptical binaries [141–143].

A. Elliptical orbits

Before presenting the results for elliptical orbits, we emphasize that two distinct mechanisms influence the buildup of nonlinear memory. First, it is directly affected by additional terms arising from DM environmental effects in the nonlinear memory expression [Eq. (40)]. Second, it is indirectly affected through the total inspiral time of the binary system. Both mechanisms act to enhance the nonlinear memory. However, increasing the DM parameter α simultaneously shortens the inspiral time as shown in the Table (II) while amplifying the instantaneous memory contribution. As a result, the nonlinear memory increases only up to certain values of α

TABLE II: Total inspiral time (in years) for different values of initial eccentricities e_0 and semi-latus rectum p_0 in vacuum and DM spike (α) environments. All distances are expressed in units of the ISCO scale of the IMBH.

Vacuum					
$e_0 \setminus p_0$	50	70	100	120	150
0.1	1.2	4.7	19.7	40.9	99.7
0.5	1.4	5.3	22.2	46.0	112.4
0.9	3.2	12.3	51.3	106.4	259.8

DM ($\alpha = 2.25$)					
$e_0 \setminus p_0$	50	70	100	120	150
0.1	3.8	10.6	24.8	35.3	51.1
0.5	4.2	11.2	25.1	35.0	49.8
0.9	6.9	14.6	26.3	33.4	43.3

DM ($\alpha = 2.35$)					
$e_0 \setminus p_0$	50	70	100	120	150
0.1	2.0	3.9	7.0	9.1	12.1
0.5	2.1	4.0	7.0	9.0	11.9
0.9	2.6	4.4	7.0	8.6	10.8

DM ($\alpha = 2.5$)					
$e_0 \setminus p_0$	50	70	100	120	150
0.1	0.3	0.4	0.7	0.8	1.1
0.5	0.3	0.4	0.7	0.8	1.1
0.9	0.3	0.5	0.8	1.0	1.2

and the initial binary parameters. Beyond this regime, even though a larger α tends to strengthen the memory contribution, the reduced inspiral time prevents the total accumulated memory from exceeding that of the vacuum case. Note that, for most of the inspiral cases considered in this work, we focus on elliptical binaries whose orbital evolution requires more than one year to reach the LSO, considering the long observation period of LISA.

1. Memory evolution vs eccentricity

For elliptical orbits, we compute the dominant nonlinear memory modes $h_{20}^{(\text{mem})}$ and $h_{40}^{(\text{mem})}$ as functions of the orbital eccentricity. The results are shown in Figs. (2a), (2b), and (2c), corresponding to different values of initial eccentricity e_0 , the initial semi-latus rectum p_0 , and the DM spike exponent α , respectively. As illustrated in Fig. (2a), a larger initial eccentricity leads to a slightly enhanced nonlinear memory, consistent with the hereditary nature of the memory effect. Fig. (2b) demonstrates that increasing the initial semi-latus rectum p_0 results in a marginally larger nonlinear memory amplitude and a longer inspiral duration prior to reaching the LSO. Fi-

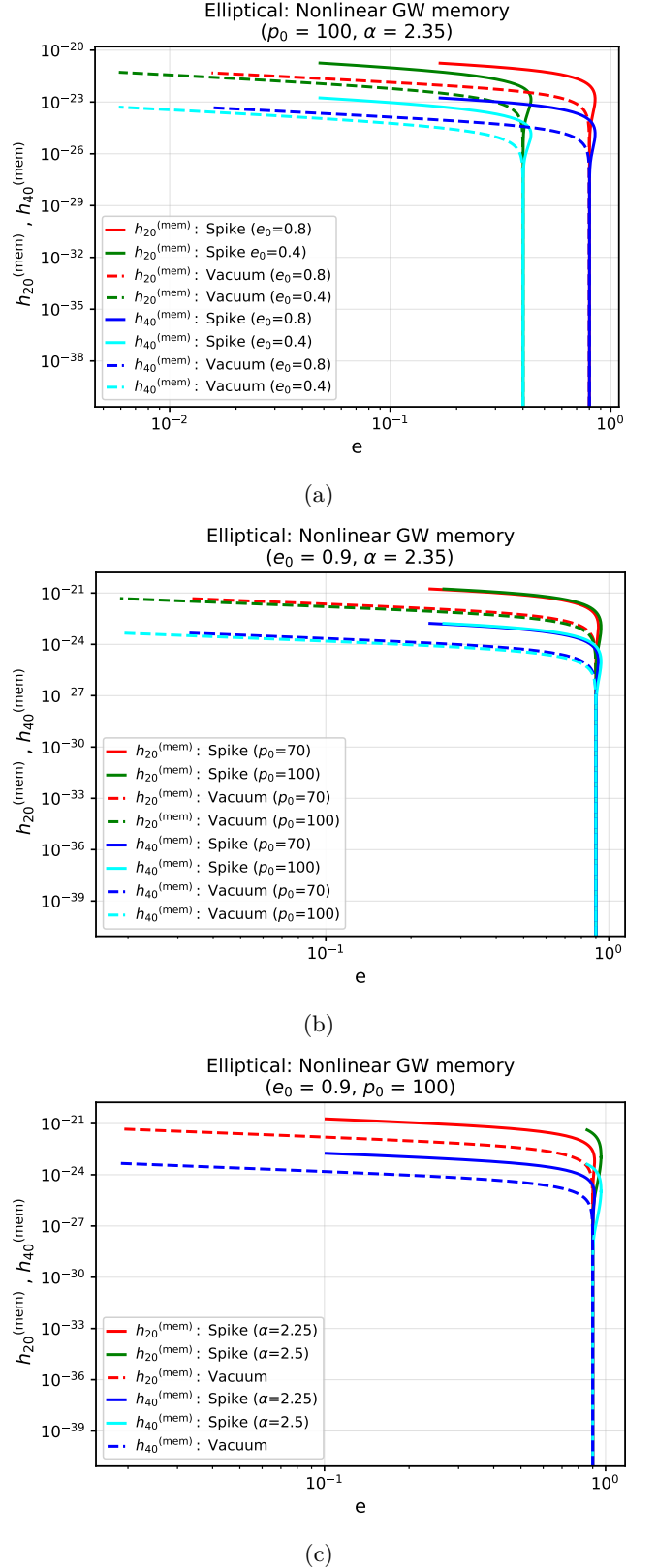


FIG. 2: The above plots show the $h_{20}^{(\text{mem})}$ and $h_{40}^{(\text{mem})}$ as functions of eccentricity with different values of initial eccentricities e_0 , initial semi-latus rectum p_0 and DM spike exponent α in panels (a), (b), and (c), respectively, for elliptical binaries. We also consider $R = 10\text{Mpc}$.

nally, Fig. (2c) shows the dependence of nonlinear memory on the DM spike exponent α : a larger value, $\alpha = 2.5$, leads to more rapid orbital evolution and reduced time for memory accumulation, causing earlier truncation of the memory signal, whereas a smaller value, $\alpha = 2.25$, allows for a slower inspiral and consequently a greater overall buildup of nonlinear memory.

In Fig. (3), we compare the impact of DM spike and NFW density profiles on the nonlinear memory relative to the vacuum case. We find that the spike profile produces a significantly larger instantaneous memory amplitude than either the NFW profile or the vacuum. However, the total accumulated memory by the time the system reaches the LSO is comparable for all these three cases. This behavior arises because binaries embedded in a spike environment experience a shorter inspiral time due to stronger environmental effects on binary motion. In contrast, the NFW profile has a much weaker influence on the orbital evolution, leading to nearly the same orbital parameter changes as in the vacuum case, but with a longer inspiral time. Consequently, although the instantaneous memory amplitude is smaller for the NFW profile, its longer inspiral duration allows for comparable cumulative memory growth prior to the LSO.

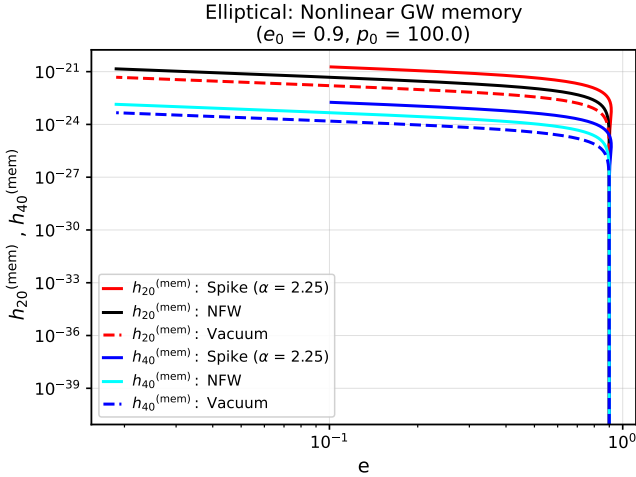


FIG. 3: Comparison of nonlinear memory modes from elliptical binaries as functions of eccentricity in vacuum and in DM environments. The $(2, 0)$ and $(4, 0)$ modes are shown for a spike profile ($\alpha = 2.25$) and an NFW halo for binaries with $e_0 = 0.9$ and $p_0 = 100$.

2. Detectability of nonlinear memory due to DM

To assess detectability, we compute the SNR of waveforms constructed with and without nonlinear memory, for binaries evolving in vacuum and in a DM spike environment. The GW polarizations are obtained from the

mode decomposition of Eq. (4), truncated at $\ell = 2$:

$$\begin{aligned} h_+ - ih_\times &\approx \sum_{m=-2}^2 H_{2m} Y_{2m}(\Theta, \Phi), \\ &= H_{20} Y_{20} + H_{2+2} Y_{2+2} + H_{2-2} Y_{2-2}, \end{aligned} \quad (57)$$

where $H_{lm} = h_{lm}^N$ (excluding memory) or $H_{lm} = h_{lm}$ (including memory), as defined in Eq. (6), $\{2\pm 1\}$ modes satisfy $h_{2\pm 1}^N = 0 \implies H_{2\pm 1} = 0$ from Eq. (9) and Y_{lm} denote spin-weighted spherical harmonics, $\Theta = \pi/3$ is the inclination angle (defined as the angle between the orbital angular momentum (the z-axis of our coordinate system) and the line of sight to the observer) taken, and Φ is the coalescence phase. Using this, the detector response is obtained by projecting the polarizations onto the antenna pattern functions [144],

$$h(t) = F_+(t)h_+(t) + F_\times(t)h_\times(t). \quad (58)$$

The SNR is computed in the time domain as

$$\rho_{\text{signal}} = \sqrt{2 \int_{t_{\text{init}}}^{t_{\text{LSO}}} \frac{h^2(t)}{S_h(\nu(t))} dt}, \quad (59)$$

where $S_h(\nu)$ is the one-sided noise power spectral density (PSD) of the detector, $\nu(t)$ is the instantaneous GW frequency and integration is performed from an initial reference time (t_{init}) up to the LSO (t_{LSO}). Since the waveform $h(t)$ is obtained numerically, performing a direct Fourier transform of the discretized time-domain waveform to obtain GW frequency introduces numerical artifacts. To mitigate this issue, we restrict our analysis to low-eccentricity orbits, for which the instantaneous GW frequency can be approximated as:

$$\nu(t) = \frac{1}{\pi} \frac{d\phi}{dt}. \quad (60)$$

For LISA, we adopt the noise model from [144],

$$\begin{aligned} S_h(\nu(t)) = \min & \left[\frac{S_h^{\text{inst}}(\nu)}{\exp(-\beta T_{\text{mission}}^{-1} dN/d\nu)} + S_h^{\text{exgal}}(\nu), \right. \\ & \left. S_h^{\text{inst}}(\nu) + S_h^{\text{gal}}(\nu) + S_h^{\text{exgal}}(\nu) \right], \end{aligned} \quad (61)$$

where

$$\begin{aligned} S_h^{\text{inst}}(\nu) &= 9.18 \times 10^{-52} \nu^{-4} + 1.59 \times 10^{-42} + \\ & \quad 9.18 \times 10^{-38} \nu^2 \text{ Hz}^{-1}, \\ S_h^{\text{gal}}(\nu) &= 2.1 \times 10^{-45} \left(\frac{\nu}{1 \text{ Hz}} \right)^{-7/3} \text{ Hz}^{-1}, \\ S_h^{\text{exgal}}(\nu) &= 4.2 \times 10^{-47} \left(\frac{\nu}{1 \text{ Hz}} \right)^{-7/3} \text{ Hz}^{-1}, \end{aligned}$$

and $\frac{dN}{d\nu} = 2 \times 10^{-3} \left(\frac{1 \text{ Hz}}{\nu} \right)^{11/3}$ and $\beta T_{\text{mission}}^{-1} = 1.5/\text{yr}$ are taken from [144].

For GWSat, we use the PSD model of Ref. [145],

$$S_h(\nu) = (10^{-25} \nu^{-2} + 10^{-23} + 10^{-24} \nu^{-1})^2 \text{ Hz}^{-1}. \quad (62)$$

We evaluate the SNR for four cases: (i) vacuum without memory, (ii) vacuum including memory, (iii) DM spike without memory, and (iv) DM spike including memory. The results are presented in Fig. (4). For binaries evolving in a vacuum, the inclusion of nonlinear memory results in a slight increase in the SNR relative to the case without memory. However, the SNR in both vacuum cases (i) and (ii) is generally larger than that for binaries embedded in a DM spike environment, reflecting the faster inspiral and reduced signal duration induced by environmental effects. Nevertheless, in all cases considered, the resulting SNR values remain at levels that may be detectable by LISA and GWSat.

3. Effect of DM on memory detection

To examine the impact of environmental effects on the detectability of nonlinear memory, we compute the SNR of the memory-only signal for binaries evolving in a vacuum and in a DM spike environment for different values of the spike index α . The memory signal is constructed by projecting the nonlinear memory polarizations onto the detector antenna-pattern functions. The polarizations include only the dominant $m = 0$ memory modes, $h_{20}^{(\text{mem})}$ and $h_{40}^{(\text{mem})}$, and are given by

$$h_{+}^{(\text{mem})}(e(t), \Theta) = \frac{1}{8} \sqrt{\frac{30}{\pi}} \sin^2 \Theta \left[h_{20}^{(\text{mem})} + \frac{\sqrt{3}}{2} h_{40}^{(\text{mem})} (7 \cos^2 \Theta - 1) \right],$$

$$h_{\times}^{(\text{mem})}(e(t), \Theta) = 0.$$

The results, shown in Fig. (5), indicate that for certain values of α , the SNR of the memory signal in a DM spike environment exceeds that of the vacuum case, suggesting that environmental effects can enhance the detectability of nonlinear memory. However, this conclusion depends on the chosen initial orbital parameters ($e_0 = 0.1$, $p_0 = 50$). More generally, memory detectability may be enhanced only for specific combinations of initial parameters (e_0 , p_0) and the spike index α . In particular, increasing α enhances the instantaneous memory amplitude but reduces the total accumulated memory due to the shortened inspiral time (for fixed e_0 and p_0), leading to a nontrivial dependence of detectability on α .

4. Effect of memory on detection of DM around IMBH

To see the counter effect of nonlinear memory on the detection of a DM medium around an IMBH, we compute the mismatch between waveforms generated in a DM spike environment with and without memory. The analysis is done in two ways: (i) the mismatch accumulated month-by-month during the final year prior to the LSO, shown in Fig. (6a), and (ii) the mismatch of the

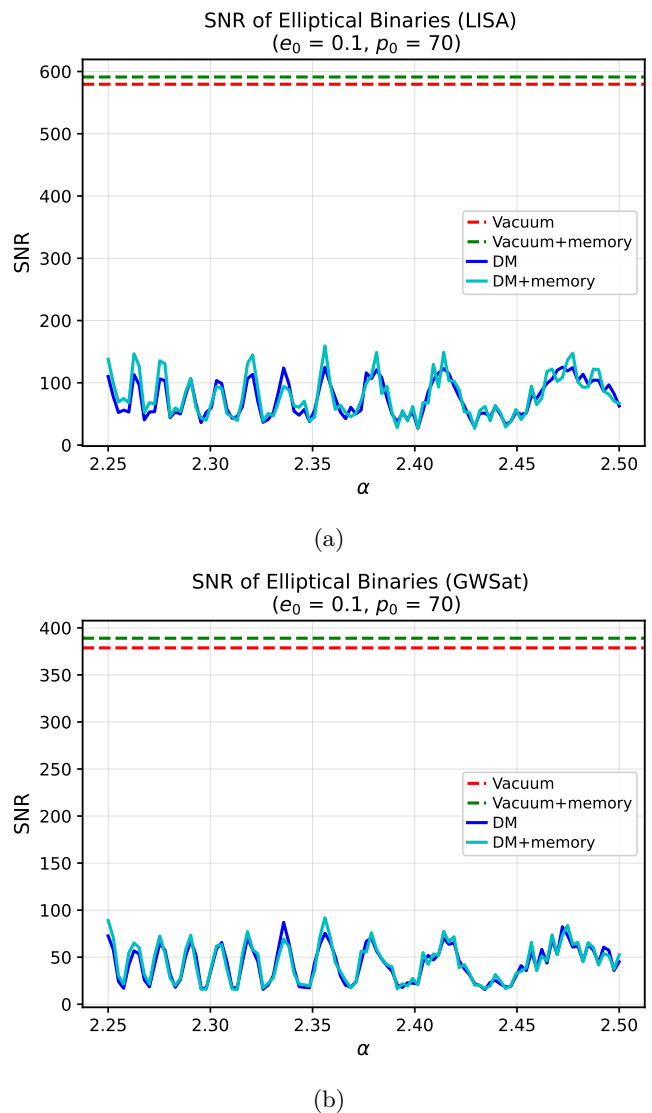
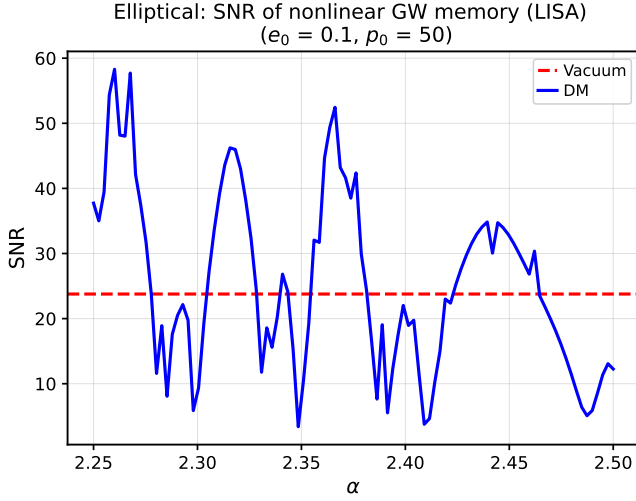


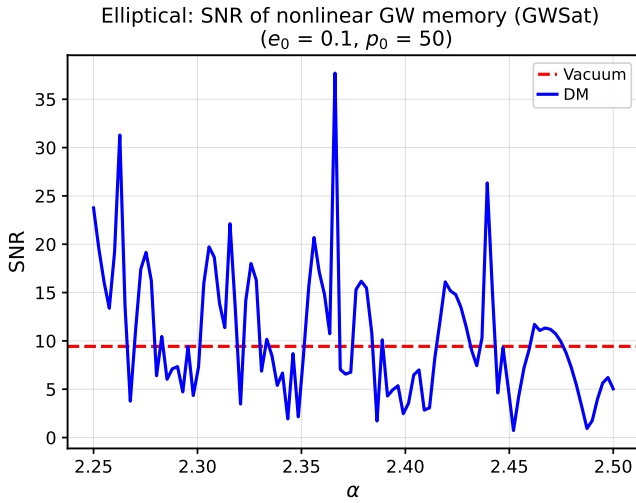
FIG. 4: SNR of GW signal from elliptical binaries as a function of the DM spike exponent α . Panel (a) shows the SNR computed for the LISA detector, while panel (b) shows the corresponding results for GWSat. In each panel, four cases are considered: binaries evolving in a vacuum, binaries in a vacuum with nonlinear memory, binaries embedded in a DM environment, and DM binaries with nonlinear memory. The initial orbital parameters are fixed to $e_0 = 0.1$ and $p_0 = 70$ with $R = 10\text{Mpc}$.

full accumulated signal as a function of the DM spike exponent α , shown in Fig. (6b). To find mismatch between signals h_1 and h_2 , we use:

$$\mathcal{M} = 1 - \mathcal{O}(h_1, h_2), \quad (63)$$



(a)



(b)

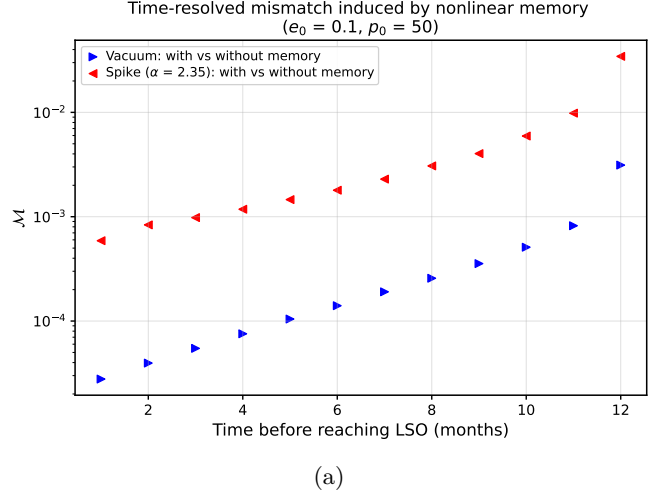
FIG. 5: SNR of the nonlinear memory response from elliptical binaries as a function of the DM spike exponent α , computed using the (2, 0) and (4, 0) memory modes, which are combined to construct the memory polarizations and projected onto the detector response. Results are shown for LISA (a) and GWSat (b), assuming $e_0 = 0.1$ and $p_0 = 50$, for vacuum and DM spike environment.

where $\mathcal{O}(h_1, h_2)$ is the overlap between the signals h_1 and h_2 , written as:

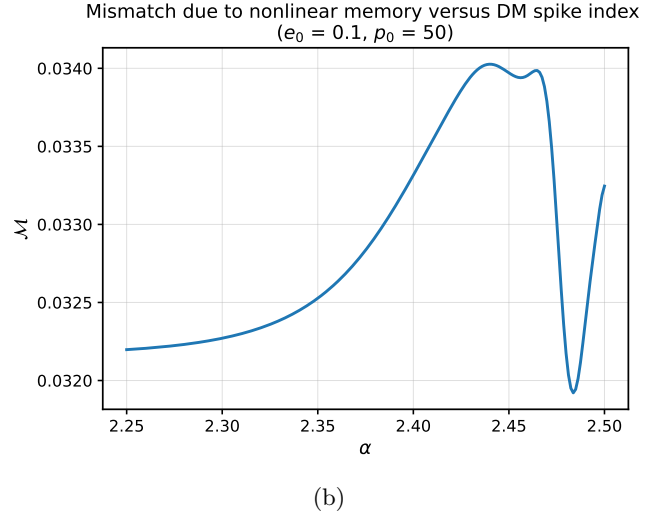
$$\mathcal{O}(h_1, h_2) = \frac{(h_1, h_2)}{\sqrt{(h_1, h_1)(h_2, h_2)}}, \quad (64)$$

and

$$(h_1, h_2) = 4\text{Re} \int_{f_{\text{initial}}}^{f_{\text{final}}} \frac{\tilde{h}_1(f)\tilde{h}_2^*(f)}{S_n(f)} df, \quad (65)$$



(a)



(b)

FIG. 6: Mismatch induced by nonlinear memory in elliptical binaries evolving in vacuum and in a DM environment. In panel (a), we show the time-resolved mismatch between waveforms computed with and without nonlinear memory, evaluated over successive monthly segments during the final year of evolution prior to the LSO. In panel (b), we show the mismatch computed using the full accumulated signal, as a function of the DM spike exponent α . In all cases, the waveforms are constructed using the SPA for low-eccentricity orbits, and the comparison isolates the impact of nonlinear memory by toggling its contribution while keeping all other parameters fixed. Results are shown for binaries with $e_0 = 0.1$ and $p_0 = 50$.

where $\tilde{h}_1(f)$ and $\tilde{h}_2(f)$ are signals in frequency domain which are obtained using the SPA [141–143] for low eccentricity elliptical orbit, and $S_n(f)$ is the LISA noise PSD used in the mismatch analysis.

We find that the inclusion of nonlinear memory leads to a substantial increase in mismatch for binaries embedded in a DM spike, reaching values of order $\mathcal{O}(10^{-3})$

to $\mathcal{O}(10^{-1})$ as the system approaches the LSO (see Fig. (6a)). A similar, though generally smaller, increase is also observed for binaries evolving in vacuum. Fig. (6b) shows that the full-signal mismatch in the DM case increases with α up to a certain value. This dependence is nontrivial and sensitive to the initial orbital parameters (e_0, p_0) as well as the spike index α . Nevertheless, in all such cases, the memory-induced mismatch is large enough to motivate a dedicated parameter-estimation analysis.

B. Hyperbolic orbits

In this section, we present results for the nonlinear memory for unbounded (hyperbolic) binaries embedded in a DM environment. We first examine the dependence of the memory amplitude on the initial orbital parameters (e_0, p_0) and the DM spike exponent α , as shown in Fig. (7). We then compare the effects of a DM spike and an NFW profile relative to the vacuum case in Fig. (8). In all scenarios considered, the presence of a DM environment enhances the nonlinear memory compared to the vacuum. However, the memory amplitude remains small, at $\mathcal{O}(10^{-26})$, making its detection extremely challenging even for future space-based detectors such as LISA and GWSat.

1. Dependency on orbital parameters

Fig. (7) presents the dominant nonlinear memory modes, $h_{20}^{(\text{mem})}$ and $h_{40}^{(\text{mem})}$, as functions of the true anomaly for hyperbolic binaries evolving in a DM spike environment and in vacuum. We find that the nonlinear memory generated during hyperbolic encounters is strongly suppressed, reaching amplitudes of order $\mathcal{O}(10^{-26})$. Such small amplitudes would be challenging to detect even with the proposed future GW detectors. Nevertheless, in all cases considered, the nonlinear memory in the presence of a DM spike remains larger than that obtained in the vacuum case.

Here, the *vacuum case* includes only PN corrections from GR up to 2.5PN order, whereas the *DM case* incorporates additional environmental effects such as DF, accretion, and the gravitational potential of the DM distribution, on top of the same PN corrections.

We further observe a clear dependence on the initial orbital parameters, including the eccentricity e_0 and the semi-latus rectum p_0 , which is related to the impact parameter of the hyperbolic orbit. As shown in Figs. (7a) and (7b), larger e_0 leads to slightly enhanced nonlinear memory. In contrast, smaller values of p_0 produce a significantly larger memory signal compared to the corresponding vacuum case with identical orbital parameters.

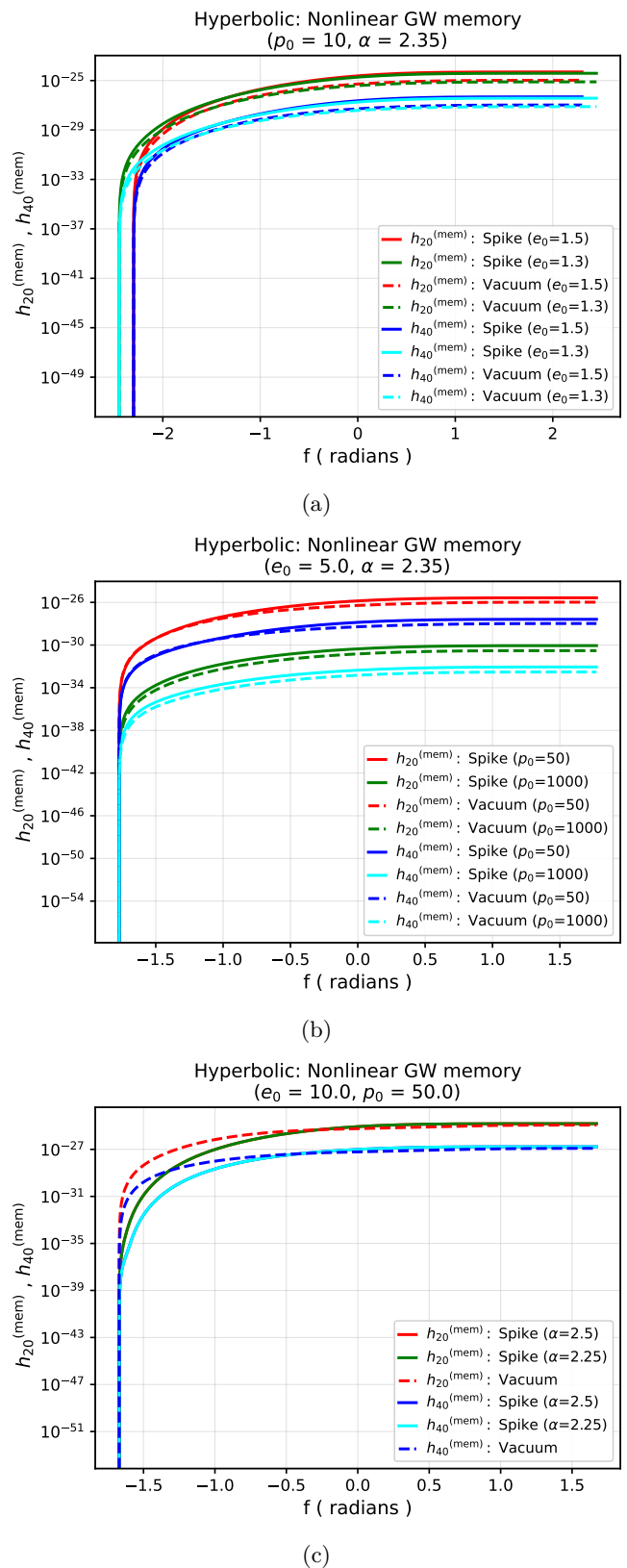
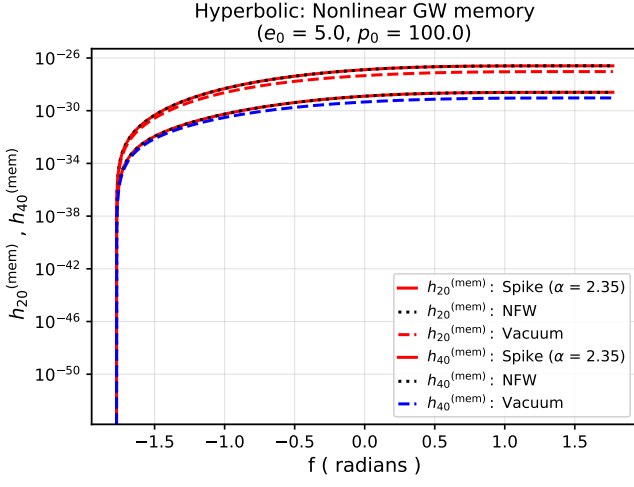
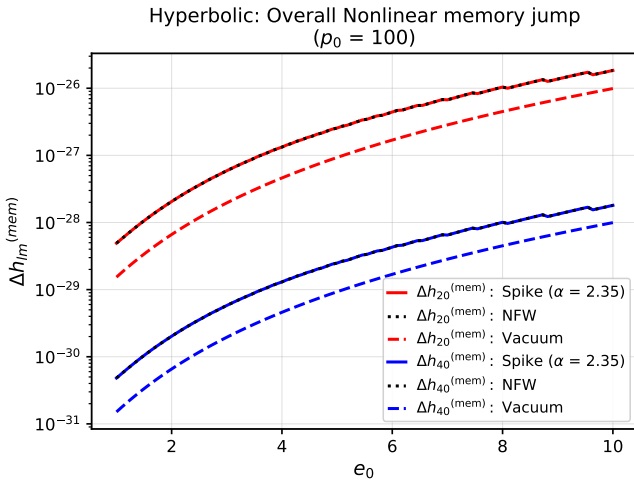


FIG. 7: The above plots show the $h_{20}^{(\text{mem})}$ and $h_{40}^{(\text{mem})}$ as functions of true anomaly with different values of initial eccentricities e_0 , initial semi-latus rectum p_0 and DM spike exponent α in panels (a), (b), and (c) respectively for hyperbolic binaries.



(a)



(b)

FIG. 8: The top panel (a) shows the $h_{20}^{(\text{mem})}$ and $h_{40}^{(\text{mem})}$ as functions of true anomaly for hyperbolic binaries in a DM spike, NFW, and in vacuum. The panel (b) below shows the overall nonlinear jump for hyperbolic binaries as a function of initial eccentricity.

2. Dependency on DM spike exponent

Fig. (7c) illustrates the effect of the DM density power-law exponent α on the nonlinear memory from a hyperbolic binary, with e_0 and p_0 held fixed. For the range of α values considered, the nonlinear memory curves nearly overlap, indicating a weak dependence on α . At early stages of the encounter, the nonlinear memory in the presence of DM is slightly smaller than that in vacuum; however, as the orbit evolves, it becomes marginally larger than the vacuum result.

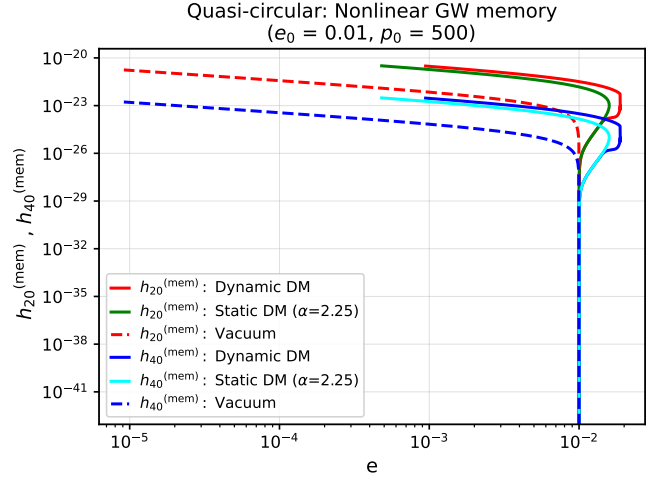


FIG. 9: The above plot shows $h_{20}^{(\text{mem})}$ and $h_{40}^{(\text{mem})}$ nonlinear memory modes as functions of eccentricity due to quasi-circular binaries. The dashed line represents the memory in vacuum, accounting only for GW backreaction. The solid red line includes the effects of a dynamically evolving DM spike through DF apart from GW backreaction, while the solid green line corresponds to a static DM spike profile.

3. Comparison: DM Spike, NFW & Vacuum

In Fig. (8), we show the nonlinear memory and the overall memory jump from hyperbolic binaries in the presence of a DM spike, an NFW profile, and in vacuum, plotted in Figs. (8a) and (8b), respectively. From Fig. (8a), we see that the nonlinear memory grows with true anomaly and is consistently higher in the presence of DM compared to vacuum, while the results for the DM spike and NFW profile nearly overlap. Fig. (8b) further shows that the memory jump is significantly larger than in vacuum and increases with initial eccentricities. However, the curves for the DM spike and NFW profile remain almost overlapping, suggesting that different DM environments have a nearly similar effect on the nonlinear memory from hyperbolic binaries.

C. Quasi-circular orbits

In Fig. (9), we show the nonlinear memory from a quasi-circular binary as a function of eccentricity in the presence of both static and dynamic DM spike environments. In both cases, the memory amplitude is larger than in vacuum, with the dynamic DM case yielding slightly higher values than the static case. Moreover, the memory buildup in the dynamic case is truncated earlier, reflecting the faster orbital decay driven by DF in the evolving DM environment in addition to GW backreaction.

V. DISCUSSION

Nonlinear GW memory is a hereditary effect; it depends on the cumulative radiated energy and encodes the past evolution of the source rather than only its instantaneous configuration. This makes it a natural observable to probe long-lived environmental effects. Motivated by this feature, in this work we studied how DM environments surrounding IMBHs modify the leading-order nonlinear memory generated by non-spinning intermediate-mass-ratio binaries. Our analysis focused on elliptical, hyperbolic, and quasi-circular configurations, with the orbital dynamics evolved using the osculating-orbit method in the presence of DM gravity, DF, accretion, and GW backreaction. Our main result is that DM environments can reshape the buildup of nonlinear memory by altering the orbital evolution of the binary. In this sense, the environment affects the memory both directly, through the modified source dynamics entering the memory integrand, and indirectly, through changes in the duration of the orbital evolution over which the hereditary contribution accumulates. The relative importance of these effects depends strongly on the orbital class and on the properties of the DM profile. We now briefly summarize the findings of our analysis for the various orbital classes:

- For **elliptical binaries**, we find that the memory grows monotonically as the orbit circularizes, but the cumulative amplitude at the end of the inspiral is modified in a nontrivial way by the surrounding DM distribution. In a minispikes environment, steeper spikes increase the strength of environmental forces and can enhance the instantaneous memory contribution. At the same time, they also accelerate the inspiral and reduce the accumulation time available before the LSO. The resulting competition implies that the total memory does not vary monotonically with the spike exponent α . Instead, for fixed orbital parameters, the memory, the memory-only SNR, and the memory-induced mismatch can all show parameter-dependent local extrema. These features should therefore be interpreted as reflecting a competition between stronger instantaneous environmental forcing and shorter inspiral duration, rather than as universal signatures of the model.

The dependence on the initial orbital parameters follows the same logic. Larger initial eccentricities and larger initial semi-latus recta generally allow more time for hereditary buildup and hence tend to increase the accumulated memory. However, this tendency can be partially counteracted by environmental effects, especially for steeper minispikes that shorten the inspiral substantially. Our comparison between minispikes, NFW, and vacuum cases further shows that a spike can produce a larger instantaneous memory than either vacuum

or NFW, while the final accumulated memory may remain comparable because the stronger environment also drives a faster inspiral.

- For **hyperbolic binaries**, the situation is qualitatively different. Although the DM environment enhances the nonlinear memory relative to the vacuum case, the overall amplitude remains very small, typically of order $\mathcal{O}(10^{-26})$ in the cases considered here. This makes direct detection highly challenging even for future space-based detectors. We also find that the overall memory jump is modified by the presence of the environment, but within the present setup the spike and NFW profiles produce quantitatively similar effects. Thus, while hyperbolic encounters remain useful for illustrating how environments modify the nonlinear memory jump, they appear much less promising observationally than the elliptical systems studied here.
- For **quasi-circular binaries**, we considered both a static minispikes and an empirical prescription for an evolving effective density profile. In both cases, the nonlinear memory is enhanced relative to vacuum. The evolving profile leads to a modestly larger memory amplitude than the static case, but the buildup terminates earlier because the inspiral proceeds faster under the combined action of GW backreaction and DF. Compared to the elliptical case, the quasi-circular setup provides a cleaner secular picture, though the quantitative results remain model-dependent because of the empirical nature of the evolving-density prescription.
- We also used the computed waveforms to estimate representative SNRs and mismatches in the context of space-based detectors such as LISA and GWSat. These estimates suggest that, for low-eccentricity elliptical binaries, nonlinear memory can leave a noticeable imprint on the waveform in the parameter ranges considered here. At the same time, the present detection-related results should be interpreted with appropriate caution. The SNR and mismatch calculations are intended as representative, order-of-magnitude estimates within an approximate low-eccentricity framework, rather than as a full data-analysis forecast. In particular, the detailed dependence of the memory-only SNR and the mismatch on α is sensitive to the choice of initial orbital parameters, and localized enhancements in these curves should be viewed as parameter-specific crossover features rather than generic predictions.

The broader implication of our analysis is therefore not that nonlinear memory provides the dominant observational probe of DM environments, but rather that it offers a complementary one. Environmental effects are generally expected to be more prominent in the oscillatory sector of the waveform, especially through their imprint

on the orbital phase evolution. However, because nonlinear memory is hereditary, it responds to the integrated history of that evolution and can therefore encode environmental information in a qualitatively distinct manner. From this perspective, the memory sector may offer an additional handle on the long-timescale influence of DM surrounding IMBHs.

To our knowledge, this work provides the first systematic study of how DM environments modify leading-order nonlinear GW memory from intermediate-mass-ratio binaries. The main lesson is that the surrounding medium can imprint itself on the hereditary sector of the waveform in ways that are subtle, orbit-dependent, and often non-monotonic. While a full assessment of observational prospects will require more refined waveform modeling and parameter-estimation tools, the present results provide an order-of-magnitude foundation for exploring nonlinear memory as a complementary probe of astrophysical environments around IMBHs.

Further, our analysis incorporates several simplifying assumptions: leading-order nonlinear memory corrections to the waveform, small perturbative effects from the environment on the binary dynamics, a static DM profile for elliptical and hyperbolic orbits, and non-spinning binary components. These assumptions define the scope of the current study and highlight several directions for future work. Relaxing each of these assumptions can give us a more detailed study of this interplay, specifically including non-trivial effects of disks [146], where motions can also have intricate effects on their detection prospects [147]. It would be interesting to incorporate such features into our future analysis to better model the waveforms. Further, one can also perform the Fisher analysis in our context to infer the degeneracy or correlation among binary black hole parameters, including environmental effects on nonlinear memory [68]. Also, studying the effects of the medium in relativistic binaries embedded in a dynamically evolving DM environment through N -body simulations [125] will be a great way to push this line of study. Such systems may yield a substantially larger memory contribution to the waveform and offer improved detection prospects, especially with next-generation space-based detectors. Additionally, such analyses can be extended to spinning binaries with generic orbits [148] and to compact binaries

exhibiting non-equatorial eccentric motion (inclined orbits). These scenarios are relevant and also realistic for more robust waveform modeling in the context of future detectors. We hope to address some of these aspects in our future studies.

ACKNOWLEDGEMENTS

The research of S.K. is funded by National Post-Doctoral Fellowship (Grant No. PDF/2023/000369) from the ANRF (formerly SERB), Department of Science and Technology (DST), Government of India. AC is funded by Beijing Natural Science Foundation (BNSF) International Scientists Project (Grant No. IS25033) and also from a postdoctoral fellowship (Grant No. 202504) through the Department of Astronomy, Tsinghua University. A.C. would also like to acknowledge the support of European Union's Horizon Europe research and innovation programme under grant agreement No 101131928, project ACME. A.B. is supported by the Core Research Grant (CRG/2023/005112) by the Department of Science and Technology Science and Anusandhan National Research Foundation (formerly SERB), Government of India. A.B. thank the speakers of "Testing Aspects General Relativity-IV" for the illuminating discussion. A.B. also acknowledges the associateship program of the Indian Academy of Science, Bengaluru. R.K.S. acknowledges the support in part by the International Center for Theoretical Sciences (ICTS) for participating in the program Beyond the Horizon: Testing the black hole paradigm (code: ICTS/BTH2025/03). Authors also acknowledge Srijit Bhattacharjee, Abhishek Sharma and Divya Tahelyani for useful discussions.

Appendix A: Equations for the case of NFW

The perturbed Newtonian binary in case of NFW profile is given as:

$$\ddot{\vec{r}} = -\frac{M}{r^2}\hat{n} + \vec{f}_{\text{DM}} + \vec{f}_{\text{DF}} + \vec{f}_{\text{acc}} + \vec{f}_{2.5\text{PN}}. \quad (\text{A1})$$

This equation can be resolved into the equations for r and ϕ as:

$$\begin{aligned} \ddot{r} &= r\dot{\phi}^2 - \frac{M}{r^2} - \frac{M_{\text{DM}}(r)}{r^2} - \frac{4\pi m_2 \rho_{\text{DM}}(I_v \xi(v) + \lambda)\dot{r}}{v^3} - \frac{M}{r^2} [A_{2.5\text{PN}} + \dot{r}B_{2.5\text{PN}}], \\ \ddot{\phi} &= -\frac{2\dot{r}\dot{\phi}}{r} - \frac{4\pi m_2 \rho_{\text{DM}}(I_v \xi(v) + \lambda)\dot{\phi}}{v^3} - \frac{M}{r} [B_{2.5\text{PN}}]\dot{\phi}, \end{aligned} \quad (\text{A2})$$

where, $M_{\text{DM}}(r)$ is the mass of NFW DM (given in sec-

tion (III A 1)) as function of distance r and NFW profile ρ_{DM} mentioned in Eq. (2).

-
- [1] B. P. Abbott et al. (LIGO Scientific, Virgo), *Phys. Rev. Lett.* **116**, 061102 (2016), 1602.03837.
- [2] B. P. Abbott et al. (LIGO Scientific, Virgo), *Phys. Rev. Lett.* **116**, 241102 (2016), 1602.03840.
- [3] B. P. Abbott et al. (LIGO Scientific, Virgo), *Phys. Rev. Lett.* **116**, 241103 (2016), 1606.04855.
- [4] B. P. Abbott et al. (LIGO Scientific, VIRGO), *Phys. Rev. Lett.* **118**, 221101 (2017), [Erratum: *Phys.Rev.Lett.* 121, 129901 (2018)], 1706.01812.
- [5] B. P. Abbott et al. (LIGO Scientific, Virgo), *Phys. Rev. Lett.* **123**, 011102 (2019), 1811.00364.
- [6] Y. B. Zel'dovich and A. G. Polnarev, *Sov. Astron.* **18**, 17 (1974).
- [7] V. B. Braginsky and L. P. Grishchuk, *Sov. Phys. JETP* **62**, 427 (1985).
- [8] V. B. Braginsky and K. S. Thorne, *Nature* **327**, 123 (1987).
- [9] D. Christodoulou, *Phys. Rev. Lett.* **67**, 1486 (1991).
- [10] K. S. Thorne, *Phys. Rev. D* **45**, 520 (1992), URL <https://link.aps.org/doi/10.1103/PhysRevD.45.520>.
- [11] M. Favata, *Phys. Rev. D* **80**, 024002 (2009), 0812.0069.
- [12] M. Favata, *Astrophys. J. Lett.* **696**, L159 (2009), 0902.3660.
- [13] M. Favata, *Class. Quant. Grav.* **27**, 084036 (2010), 1003.3486.
- [14] M. Favata, *Phys. Rev. D* **84**, 124013 (2011), 1108.3121.
- [15] A. Tolish and R. M. Wald, *Phys. Rev. D* **89**, 064008 (2014), 1401.5831.
- [16] L. Bieri and D. Garfinkle, *Phys. Rev. D* **89**, 084039 (2014), URL <https://link.aps.org/doi/10.1103/PhysRevD.89.084039>.
- [17] A. Hait, S. Mohanty, and S. Prakash, *Phys. Rev. D* **109**, 084037 (2024), 2211.13120.
- [18] N. Jokela, K. Kajantie, and M. Sarkkinen, *Phys. Rev. D* **106**, 064022 (2022), URL <https://link.aps.org/doi/10.1103/PhysRevD.106.064022>.
- [19] P. D. Lasky, E. Thrane, Y. Levin, J. Blackman, and Y. Chen, *Phys. Rev. Lett.* **117**, 061102 (2016), 1605.01415.
- [20] C. Talbot, E. Thrane, P. D. Lasky, and F. Lin, *Phys. Rev. D* **98**, 064031 (2018), 1807.00990.
- [21] K. Islo, J. Simon, S. Burke-Spolaor, and X. Siemens (2019), 1906.11936.
- [22] O. M. Boersma, D. A. Nichols, and P. Schmidt, *Phys. Rev. D* **101**, 083026 (2020), 2002.01821.
- [23] A. M. Grant and D. A. Nichols, *Phys. Rev. D* **107**, 064056 (2023), [Erratum: *Phys.Rev.D* 108, 029901 (2023)], 2210.16266.
- [24] N. Afshordi et al. (LISA Consortium Waveform Working Group) (2023), 2311.01300.
- [25] B. Goncharov, L. Donnay, and J. Harms, *Phys. Rev. Lett.* **132**, 241401 (2024), 2310.10718.
- [26] S. Sun, C. Shi, J.-d. Zhang, and J. Mei, *Phys. Rev. D* **107**, 044023 (2023), 2207.13009.
- [27] A. Strominger, *Lectures on the infrared structure of gravity and gauge theory* (2018), 1703.05448, URL <https://arxiv.org/abs/1703.05448>.
- [28] P. M. Zhang, C. Duval, G. W. Gibbons, and P. A. Horvathy, *Phys. Lett. B* **772**, 743 (2017), 1704.05997.
- [29] P. M. Zhang, C. Duval, G. W. Gibbons, and P. A. Horvathy, *Phys. Rev. D* **96**, 064013 (2017), 1705.01378.
- [30] P. M. Zhang, C. Duval, and P. A. Horvathy, *Class. Quant. Grav.* **35**, 065011 (2018), 1709.02299.
- [31] I. Chakraborty and S. Kar, *Phys. Rev. D* **101**, 064022 (2020), 1901.11236.
- [32] J. Ben Achour and J.-P. Uzan, *JCAP* **08**, 004 (2024), 2406.07106.
- [33] R. Gaur (2024), 2403.07302.
- [34] M. Galoppo, R. Gaur, and C. Harvey-Hawes (2024), 2407.15289.
- [35] S. Pasterski, A. Strominger, and A. Zhiboedov, *JHEP* **12**, 053 (2016), 1502.06120.
- [36] P. Mao and X. Wu, *JHEP* **05**, 058 (2019), 1812.07168.
- [37] S. Tahura, D. A. Nichols, A. Saffer, L. C. Stein, and K. Yagi, *Phys. Rev. D* **103**, 104026 (2021), 2007.13799.
- [38] S. Hou and Z.-H. Zhu, *JHEP* **01**, 083 (2021), 2005.01310.
- [39] A. Seraj, *JHEP* **05**, 283 (2021), 2103.12185.
- [40] S. Tahura, D. A. Nichols, and K. Yagi, *Phys. Rev. D* **104**, 104010 (2021), 2107.02208.
- [41] L. Heisenberg, N. Yunes, and J. Zosso, *Phys. Rev. D* **108**, 024010 (2023), 2303.02021.
- [42] C. Ferko, G. Satishchandran, and S. Sethi, *Phys. Rev. D* **105**, 024072 (2022), URL <https://link.aps.org/doi/10.1103/PhysRevD.105.024072>.
- [43] L. Blanchet, *Living Reviews in Relativity* **17**, 2 (2014), ISSN 1433-8351, URL <https://doi.org/10.12942/lrr-2014-2>.
- [44] K. Cunningham, C. Kavanagh, A. Pound, D. Trestini, N. Warburton, and J. Neef (2024), 2410.23950.
- [45] R. A. Porto, M. M. Riva, and Z. Yang, *JHEP* **04**, 050 (2025), 2409.05860.
- [46] A. Strominger and A. Zhiboedov, *JHEP* **01**, 086 (2016), 1411.5745.
- [47] S. W. Hawking, M. J. Perry, and A. Strominger, *JHEP* **05**, 161 (2017), 1611.09175.
- [48] S. W. Hawking, M. J. Perry, and A. Strominger, *Phys. Rev. Lett.* **116**, 231301 (2016), 1601.00921.
- [49] L. Blanchet, G. Compère, G. Faye, R. Oliveri, and A. Seraj, *JHEP* **07**, 123 (2023), 2303.07732.
- [50] D. N. Solanki and S. Bhattacharjee, *Eur. Phys. J. C* **83**, 1167 (2023), 2308.02445.
- [51] D. N. Solanki and S. Bhattacharjee (2024), 2409.01783.
- [52] V. De Luca, J. Khoury, and S. S. C. Wong, *Phys. Rev. D* **112**, L021502 (2025), 2412.01910.
- [53] S. Kumar, Ph.D. thesis, IIIT, Allahabad (2021), 2203.08983.
- [54] K. Mitman, J. Moxon, M. A. Scheel, S. A. Teukolsky, M. Boyle, N. Deppe, L. E. Kidder, and W. Throwe, *Phys. Rev. D* **102**, 104007 (2020), 2007.11562.
- [55] K. Mitman et al., *Phys. Rev. D* **104**, 024051 (2021), 2105.02300.
- [56] K. Mitman et al., *Phys. Rev. D* **106**, 084029 (2022), 2208.04356.
- [57] K. Mitman et al., *Class. Quant. Grav.* **41**, 223001 (2024), 2405.08868.
- [58] L. Donnay, G. Giribet, H. A. Gonzalez, and M. Pino, *Phys. Rev. Lett.* **116**, 091101 (2016), 1511.08687.
- [59] L. Donnay, G. Giribet, H. A. González, and M. Pino, *JHEP* **09**, 100 (2016), 1607.05703.
- [60] L. Donnay, G. Giribet, H. A. González, and A. Puhm, *Phys. Rev. D* **98**, 124016 (2018), 1809.07266.

- [61] M. Blau and M. O’Loughlin, *JHEP* **03**, 029 (2016), 1512.02858.
- [62] A. A. Rahman and R. M. Wald, *Phys. Rev. D* **101**, 124010 (2020), 1912.12806.
- [63] S. Bhattacharjee, S. Kumar, and A. Bhattacharyya, *Phys. Rev. D* **100**, 084010 (2019), 1905.12905.
- [64] S. Bhattacharjee and S. Kumar, *Phys. Rev. D* **102**, 044041 (2020), 2003.09334.
- [65] S. Bhattacharjee, S. Kumar, and A. Bhattacharyya, *JHEP* **03**, 134 (2021), 2010.16086.
- [66] S. Sarkar, S. Kumar, and S. Bhattacharjee, *Phys. Rev. D* **105**, 084001 (2022), 2110.03547.
- [67] S. A. Bhat, S. Bhattacharjee, and S. J. Kapadia (2024), 2406.15604.
- [68] S. Gasparotto, R. Vicente, D. Blas, A. C. Jenkins, and E. Barausse, *Phys. Rev. D* **107**, 124033 (2023), 2301.13228.
- [69] D. Pollney and C. Reisswig, *Astrophys. J. Lett.* **732**, L13 (2011), 1004.4209.
- [70] L. Hernquist, *apj* **356**, 359 (1990).
- [71] G. Bertone, D. Hooper, and J. Silk, *Phys. Rept.* **405**, 279 (2005), hep-ph/0404175.
- [72] J. F. Navarro, C. S. Frenk, and S. D. M. White, *Astrophys. J.* **462**, 563 (1996), astro-ph/9508025.
- [73] D. Clowe, M. Bradac, A. H. Gonzalez, M. Markevitch, S. W. Randall, C. Jones, and D. Zaritsky, *Astrophys. J. Lett.* **648**, L109 (2006), astro-ph/0608407.
- [74] E. Corbelli and P. Salucci, *Mon. Not. Roy. Astron. Soc.* **311**, 441 (2000), astro-ph/9909252.
- [75] J. F. Navarro, C. S. Frenk, and S. D. M. White, *Astrophys. J.* **490**, 493 (1997), astro-ph/9611107.
- [76] P. Gondolo and J. Silk, *Phys. Rev. Lett.* **83**, 1719 (1999), astro-ph/9906391.
- [77] G. Bertone and D. Merritt, *Mod. Phys. Lett. A* **20**, 1021 (2005), astro-ph/0504422.
- [78] D. Merritt, M. Milosavljevic, L. Verde, and R. Jimenez, *Phys. Rev. Lett.* **88**, 191301 (2002), astro-ph/0201376.
- [79] P. Ullio, H. Zhao, and M. Kamionkowski, *Phys. Rev. D* **64**, 043504 (2001), astro-ph/0101481.
- [80] V. Cardoso, K. Destounis, F. Duque, R. P. Macedo, and A. Maselli, *Phys. Rev. D* **105**, L061501 (2022), 2109.00005.
- [81] K. Destounis, A. Kulathingal, K. D. Kokkotas, and G. O. Papadopoulos, *Phys. Rev. D* **107**, 084027 (2023), 2210.09357.
- [82] V. Cardoso, K. Destounis, F. Duque, R. Panosso Macedo, and A. Maselli, *Phys. Rev. Lett.* **129**, 241103 (2022), 2210.01133.
- [83] F. Duque, C. F. B. Macedo, R. Vicente, and V. Cardoso, *Phys. Rev. Lett.* **133**, 121404 (2024), 2312.06767.
- [84] Z. Shen, A. Wang, Y. Gong, and S. Yin, *Phys. Lett. B* **855**, 138797 (2024), 2311.12259.
- [85] N. Speeney, E. Berti, V. Cardoso, and A. Maselli, *Phys. Rev. D* **109**, 084068 (2024), 2401.00932.
- [86] M. Rahman, S. Kumar, and A. Bhattacharyya, *JCAP* **01**, 035 (2024), 2306.14971.
- [87] D. Tahelyani, A. Bhattacharyya, and A. S. Sengupta, *Phys. Rev. D* **111**, 083041 (2025), URL <https://link.aps.org/doi/10.1103/PhysRevD.111.083041>.
- [88] C. Zhang, G. Fu, and N. Dai, *JCAP* **04**, 088 (2024), 2401.04467.
- [89] C. F. B. Macedo, J. a. L. Rosa, and D. Rubiera-Garcia, *JCAP* **07**, 046 (2024), 2402.13047.
- [90] Y. Ravanal, G. Gómez, and N. Cruz, *Phys. Rev. D* **110**, 023027 (2024), 2404.06774.
- [91] J. C. Aurrekoetxea, J. Marsden, K. Clough, and P. G. Ferreira, *Phys. Rev. D* **110**, 083011 (2024), 2409.01937.
- [92] Y.-Z. Cheng, Y. Cao, and Y. Tang (2024), 2411.03095.
- [93] A. Chowdhuri, R. K. Singh, K. Kangsabanik, and A. Bhattacharyya, *Phys. Rev. D* **109**, 124056 (2024), URL <https://link.aps.org/doi/10.1103/PhysRevD.109.124056>.
- [94] A. Bhattacharyya, D. Ghosh, S. Ghosh, and S. Pal, *JHEP* **04**, 175 (2025), 2407.07195.
- [95] A. Bhattacharyya, D. Ghosh, S. Ghosh, and S. Pal, *JHEP* **04**, 015 (2024), 2401.05492.
- [96] D. Usseglio, D. Trestini, and A. Chowdhuri (2025), 2504.13829.
- [97] G. Cho, S. Dandapat, and A. Gopakumar, *Phys. Rev. D* **105**, 084018 (2022), 2111.00818.
- [98] A. L. Miller (2025), 2503.02607.
- [99] E. Barausse, V. Cardoso, and P. Pani, *Phys. Rev. D* **89**, 104059 (2014), URL <https://link.aps.org/doi/10.1103/PhysRevD.89.104059>.
- [100] D. Merritt, M. Milosavljević, L. Verde, and R. Jimenez, *Phys. Rev. Lett.* **88**, 191301 (2002), URL <https://link.aps.org/doi/10.1103/PhysRevLett.88.191301>.
- [101] P. Ullio, H. Zhao, and M. Kamionkowski, *Phys. Rev. D* **64**, 043504 (2001), URL <https://link.aps.org/doi/10.1103/PhysRevD.64.043504>.
- [102] E. Vasiliev and M. Zelnikov, *Phys. Rev. D* **78**, 083506 (2008), URL <https://link.aps.org/doi/10.1103/PhysRevD.78.083506>.
- [103] B. D. Fields, S. L. Shapiro, and J. Shelton, *Phys. Rev. Lett.* **113**, 151302 (2014), URL <https://link.aps.org/doi/10.1103/PhysRevLett.113.151302>.
- [104] J. Shelton, S. L. Shapiro, and B. D. Fields, *Phys. Rev. Lett.* **115**, 231302 (2015), URL <https://link.aps.org/doi/10.1103/PhysRevLett.115.231302>.
- [105] H. Zhao and J. Silk, *Phys. Rev. Lett.* **95**, 011301 (2005), URL <https://link.aps.org/doi/10.1103/PhysRevLett.95.011301>.
- [106] G. Bertone, A. R. Zentner, and J. Silk, *Phys. Rev. D* **72**, 103517 (2005), URL <https://link.aps.org/doi/10.1103/PhysRevD.72.103517>.
- [107] K. Eda, Y. Itoh, S. Kuroyanagi, and J. Silk, *Phys. Rev. Lett.* **110**, 221101 (2013), 1301.5971.
- [108] K. Eda, Y. Itoh, S. Kuroyanagi, and J. Silk, *Phys. Rev. D* **91**, 044045 (2015), 1408.3534.
- [109] X.-J. Yue and W.-B. Han, *Phys. Rev. D* **97**, 064003 (2018), URL <https://link.aps.org/doi/10.1103/PhysRevD.97.064003>.
- [110] O. A. Hannuksela, K. C. Y. Ng, and T. G. F. Li, *Phys. Rev. D* **102**, 103022 (2020), URL <https://link.aps.org/doi/10.1103/PhysRevD.102.103022>.
- [111] S. Chandrasekhar, *apj* **97**, 255 (1943).
- [112] E. C. Ostriker, *The Astrophysical Journal* **513**, 252 (1999), URL <https://dx.doi.org/10.1086/306858>.
- [113] H. Kim and W.-T. Kim, *The Astrophysical Journal* **665**, 432 (2007), URL <https://dx.doi.org/10.1086/519302>.
- [114] K. Eda, Y. Itoh, S. Kuroyanagi, and J. Silk, *Phys. Rev. Lett.* **110**, 221101 (2013), URL <https://link.aps.org/doi/10.1103/PhysRevLett.110.221101>.
- [115] N. Dai, Y. Gong, T. Jiang, and D. Liang, *Phys. Rev. D* **106**, 064003 (2022), 2111.13514.
- [116] H. Bondi and F. Hoyle, *Monthly Notices of the Royal Astronomical Society* **104**, 273 (1944), ISSN

- 0035-8711, <https://academic.oup.com/mnras/article-pdf/104/5/273/8072203/mnras104-0273.pdf>, URL <https://doi.org/10.1093/mnras/104.5.273>.
- [117] S. L. Shapiro and S. A. Teukolsky, *Black holes, white dwarfs and neutron stars. The physics of compact objects* (A Wiley-Interscience Publication, New York: Wiley, 1983, 1983).
- [118] C. F. B. Macedo, P. Pani, V. Cardoso, and L. C. B. Crispino, *Astrophys. J.* **774**, 48 (2013), 1302.2646.
- [119] X.-J. Yue, W.-B. Han, and X. Chen, *Astrophys. J.* **874**, 34 (2019), 1802.03739.
- [120] D. A. Nichols, B. A. Wade, and A. M. Grant, *Phys. Rev. D* **108**, 124062 (2023), 2309.06498.
- [121] D. Shadykul, H. Chakrabarty, and D. Malafarina (2024), 2410.18657.
- [122] A. Coogan, G. Bertone, D. Gaggero, B. J. Kavanagh, and D. A. Nichols, *Phys. Rev. D* **105**, 043009 (2022), URL <https://link.aps.org/doi/10.1103/PhysRevD.105.043009>.
- [123] Q. Alnasheet, V. Cardoso, F. Duque, and R. Panosso Macedo, *Phys. Rev. D* **112**, 044066 (2025).
- [124] V. Cardoso, C. F. B. Macedo, and R. Vicente, *Phys. Rev. D* **103**, 023015 (2021), URL <https://link.aps.org/doi/10.1103/PhysRevD.103.023015>.
- [125] T. K. Karydas, B. J. Kavanagh, and G. Bertone, *Sharpening the dark matter signature in gravitational waveforms i: Accretion and eccentricity evolution* (2024), 2402.13053, URL <https://arxiv.org/abs/2402.13053>.
- [126] M. Favata, *Journal of Physics: Conference Series* **154**, 012043 (2009), ISSN 1742-6596, URL <http://dx.doi.org/10.1088/1742-6596/154/1/012043>.
- [127] A. Laddha and A. Sen, *Phys. Rev. D* **100**, 024009 (2019), URL <https://link.aps.org/doi/10.1103/PhysRevD.100.024009>.
- [128] L. Blanchet and T. Damour, *Phys. Rev. D* **46**, 4304 (1992), URL <https://link.aps.org/doi/10.1103/PhysRevD.46.4304>.
- [129] L. Blanchet, *Class. Quant. Grav.* **15**, 113 (1998), [Erratum: *Class.Quant.Grav.* **22**, 3381 (2005)], gr-qc/9710038.
- [130] L. Blanchet and A. Le Tiec, *Classical and Quantum Gravity* **34**, 164001 (2017), URL <https://dx.doi.org/10.1088/1361-6382/aa79d7>.
- [131] M. M. Ivanov, Y.-Z. Li, J. Parra-Martinez, and Z. Zhou (2025), 2504.07862.
- [132] D. Bini, T. Damour, and A. Geralico, *Phys. Rev. D* **112**, 044028 (2025), URL <https://link.aps.org/doi/10.1103/3jhf-vdjz>.
- [133] D. Bini and T. Damour, *Phys. Rev. D* **112**, 044002 (2025), 2504.20204.
- [134] R. A. Isaacson, *Phys. Rev.* **166**, 1272 (1968), URL <https://link.aps.org/doi/10.1103/PhysRev.166.1272>.
- [135] E. Poisson and C. M. Will, *Gravity: Newtonian, Post-Newtonian, Relativistic* (Cambridge University Press, 2014).
- [136] N. Speeney, A. Antonelli, V. Baibhav, and E. Berti, *Phys. Rev. D* **106**, 044027 (2022), URL <https://link.aps.org/doi/10.1103/PhysRevD.106.044027>.
- [137] L. Blanchet, *Post-newtonian theory for gravitational waves* (2024), 1310.1528, URL <https://arxiv.org/abs/1310.1528>.
- [138] K. Glampedakis and D. Kennefick, *Phys. Rev. D* **66**, 044002 (2002), URL <https://link.aps.org/doi/10.1103/PhysRevD.66.044002>.
- [139] S. Kumar, R. K. Singh, A. Chowdhuri, and A. Bhattacharyya, *Journal of Cosmology and Astroparticle Physics* **2024**, 047 (2024), URL <https://dx.doi.org/10.1088/1475-7516/2024/10/047>.
- [140] R. K. Singh, *GitHub-nonlinear-memory: Nonlinear-gw-memory-in-astrophysical-environment*, <https://github.com/rks-circle/Nonlinear-GW-memory-in-astrophysical-environment> (2025), accessed: August 8, 2025.
- [141] C. Cutler and E. E. Flanagan, *Phys. Rev. D* **49**, 2658 (1994), gr-qc/9402014.
- [142] S. Droz, D. J. Knapp, E. Poisson, and B. J. Owen, *Phys. Rev. D* **59**, 124016 (1999), gr-qc/9901076.
- [143] T. Damour, B. R. Iyer, and B. S. Sathyaprakash, *Phys. Rev. D* **62**, 084036 (2000), gr-qc/0001023.
- [144] E. A. Huerta and J. R. Gair, *Phys. Rev. D* **84**, 064023 (2011), URL <https://link.aps.org/doi/10.1103/PhysRevD.84.064023>.
- [145] D. Tahelyani, A. Bhattacharyya, and A. S. Sengupta (2024), 2411.14063.
- [146] N. Jiang and Z. Pan, *Astrophys. J. Lett.* **983**, L18 (2025), 2503.17609.
- [147] Z. Pan, Z. Lyu, and H. Yang, *Phys. Rev. D* **104**, 063007 (2021), 2104.01208.
- [148] T. Zi and S. Kumar (2025), 2508.00516.